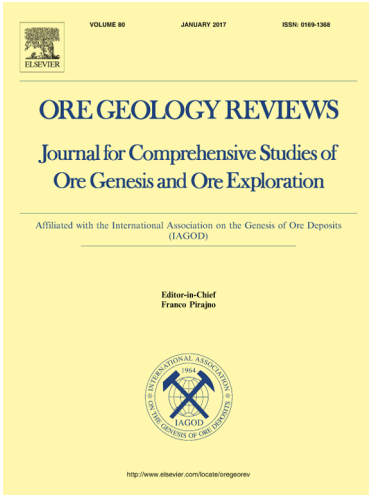

Geology, Mineralization, and Fluid Inclusion Characteristics of the Lermontovskoe Reduced-Type Tungsten (±Cu, Au, Bi) Skarn Deposit, Sikhote-Alin, Russia

Serguei G. Soloviev, Sergey.G. Kryazhev, Svetlana S. Dvurechenskaya

PII: S0169-1368(16)30501-7
DOI: http://dx.doi.org/10.1016/j.oregeorev.2017.06.002
Reference: OREGEO 2239

To appear in: *Ore Geology Reviews*

Received Date: 21 August 2016
Revised Date: 29 May 2017
Accepted Date: 2 June 2017

Please cite this article as: S.G. Soloviev, Sergey.G. Kryazhev, S.S. Dvurechenskaya, Geology, Mineralization, and Fluid Inclusion Characteristics of the Lermontovskoe Reduced-Type Tungsten (±Cu, Au, Bi) Skarn Deposit, Sikhote-Alin, Russia, *Ore Geology Reviews* (2017), doi: http://dx.doi.org/10.1016/j.oregeorev.2017.06.002

Geology, Mineralization, and Fluid Inclusion Characteristics of the Lermontovskoe Reduced-Type Tungsten (±Cu, Au, Bi) Skarn Deposit, Sikhote-Alin, Russia

Serguei G. Soloviev*, Sergey. G. Kryazhev, and Svetlana S. Dvurechenskaya****

**Int'l GeoSol Consulting Inc.*

189 – Scripps Landing N.W. Calgary, AB Canada T3L 1W1

***Russian Central Geological Prospecting Institute (TsNIGRI)*

129-B - Warshawskoe Chaussee, Moscow, Russia 113545

E-mail: serguei07@hotmail.com

Abstract

The Lermontovskoe deposit (~48Kt WO_3; average 2.6% WO_3, 0.24% Cu, 0.23 g/t Au) is situated in a W-Sn-Au metallogenic belt that formed in a collisional tectonic environment. This tungsten skarn deposit has a W-Au-As-Bi-Te-Sb signature that suggests an affinity with reduced intrusion-related Au deposits. The deposit is associated with an intrusion that is part of the ilmenite-series, high-K peraluminous granitoid (granodiorite to granite) suite. These rocks formed via mantle magma-induced melting of crustal sources.

The deposit comprises reduced-type, pyroxene-dominated prograde and retrograde skarns followed by hydrosilicate (amphibole-chlorite-pyrrhotite-scheelite-quartz) and phyllic (muscovite/sericite-carbonate-albite-quartz-scheelite-sulfide, with abundant apatite) alteration assemblages. Fluid inclusions from the skarn assemblages indicate high-temperature (>500^{o}C), high-pressure (1400-1500 bars) and high-salinity (53-60 wt.% NaCl-equiv.) magmatic-hydrothermal fluids. They were post-dated by high-carbonic, methane-dominate, low-salinity fluid at the hydrosilicate alteration stage. These fluids boiled 360-380^{o}C and 1300-1400 bars. The subsequent phyllic alteration started again with a high-temperature (>450^{o}C), high-pressure (1000-1100 bars) and high-salinity (42-47 wt.% NaCl-equiv.) fluid, with further incursion of high-carbonic, methane-dominated, low-salinity fluid that boiled at 390-420^{o}C and 1150-1200 bars. The latest phyllic alteration included the lower-temperature (340-360^{o}C), lower pressure (370-400 bars) high-carbonic, methane-dominated (but with higher CO_2 fraction), low-salinity fluid, and then the low-temperature (250-300^{o}C) H_2O-CO_2-CH_4-NaCl fluid, with both fluids boiled at the deposit level. The high-salinity aqueous fluids are interpreted to have come from crystallizing granitoid magma, whereas the reduced high-carbonic fluids probably came from a deeper mafic magma source. Both of these fluids potentially contributed to the W-Au-As-Bi-Te-Sb metal budget. Decreasing temperatures coupled with high aCa^{2+} and fluid boiling promoted scheelite deposition at all post-skarn hydrothermal stages.

The deposit is characterized by limited downdip extent of mineralized zones and abundant coarse-grained muscovite-quartz (+apatite, scheelite) aggregates that formed at the phyllic alteration stage. Together with presence of high-temperature, high-pressure and high-salinity fluids directly exsolving from

crystallizing magma, this suggests a root level of the mineralized magmatic-hydrothermal system of reduced W skarn deposits.

Keywords: reduced intrusion-related – skarn – stockwork – tungsten – gold – fluid inclusions

1. Introduction

Reduced tungsten skarns (Einaudi et al., 1981; Kwak and White, 1982) related to ilmenite-series granitoids (Ishihara, 1981) are known worldwide and include a number of large and high-grade W deposits (e.g., the MacTung and CanTung, Canada; Dick and Hodgson, 1982). They are parts of Sn-W metallogenic belts and are commonly coincident with reduced intrusion-related Au deposits (Thompson et al., 1999) in late- to post-collisional tectonic settings, and can be considered as part of a spectrum of Au-W magmatic-hydrothermal deposits (e.g., Lang and Baker, 2001; Hart, 2007). Thus studying reduced W skarn deposits is important both from the economic perspective and in the context of their possible indicatory metallogenic role.

The Lermontovskoe deposit, situated in the Primorie region of the Russian Far East, contains significant W and other (Cu, Bi, Au) mineralization. It is part of an emerging belt of reduced intrusion-related Au ($\pm$W) deposits coincident with a long-known Sn-W metallogenic belt extending along the western Pacific coast. The deposit was discovered in 1970, and since 1988 is mined by open pit. Production and current reserves total 48 Kt WO_3, with the ores averaging 2.6% WO_3 (at 0.1% WO_3 cut-off), 0.24% Cu, 0.23 g/t Au, 3.23 g/t Ag, as well as 0.5% As, 2.5% P_2O_5, and 7.06% S (Belyansky et al., 2011). Thus, although modest in size, it is a particularly high-grade W deposit.

2. Regional Tectonic and Metallogenic Setting

The Lermontovskoe deposit lies in the north-central part of the Mesozoic Sikhote-Alin orogenic system, a belt that extends for over 1200 km along the western Pacific coast and includes a series of terranes accreted to the eastern Asian continental margin during the Paleozoic and Mesozoic (Fig. 1) (e.g., Khanchuk, 2000; Khanchuk et al., 1997). Following west-dipping subduction in the Triassic-Late Jurassic, the Mesozoic

collisional processes occurred in the environment of plate sliding along large fault zones, with transform faulting led to the deposition of turbidite sequences in pull-apart basins during the Late Jurassic-Early Cretaceous. Consistently, from west to east, the Jurassic accretion prism and the Early Cretaceous turbidite terranes are distinguished (Khanchuk et al., 1997).

The main collision stage (Berriasian-Barremian) was dominated by strike-slip movements along the Central Sikhote-Alin Fault, intense thrust-faulting and folding, and emplacement of granitoid intrusions at 140-125 Ma. During the late- to post-collisional stage (Aptian-Cenomanian), movement along the Central Sikhote-Alin Fault was accompanied by development of local pull-apart basins (Kruk et al., 2014) and the most intense granitoid magmatism at 110-95 Ma in both the amalgamated Late Jurassic terranes and in the Late Jurassic-Early Cretaceous turbidite basins. The Middle Jurassic-Cenomanian collisional processes have caused tectonic piling of terrains, with corresponding development of continental crust some 30-40 km thick. Subduction re-commenced in the Late Cretaceous-Paleogene causing the formation of the Eastern Sikhote-Alin volcanic belt (Khanchuk, 2000; Khanchuk et al., 1997).

Under the late- to post-collisional tectonic regime, asthenosphere uplift through a slab window and lithosphere delamination (Khanchuk, 2000), are two possible mechanisms to explain widespread melting of crustal rocks and emplacement of granitoid suites in the Early-Late Cretaceous (Kruk et al., 2014). It is this tectonic environment, in which the Central Sikhote-Alin W-Sn-Au metallogenic province was formed. It includes numerous granite-related W and Sn deposits, which differ in composition and style of mineralization (skarn, stockwork, greisen) (Fig. 1). Tungsten-gold-base metal deposits (Vostok-2, Lermontovskoe, Skrytoe etc.) are associated with the Early Cretaceous (~111-112 to 101 Ma) high-K calc-alkaline ilmenite-series monzodiorite-granodiorite-granite plutonic suite (e.g., Rub et al., 1982; Kovalenko et al., 1988; Soloviev and Krivoschekov, 2011; Soloviev and Kryazhev, 2017; Soloviev et al., 2017). Coeval late- to post-collisional monzonitic (shoshonitic) suites (locally with coeval picrite-trachybasalt-trachyandesite volcanics; Kovalenko et al., 1988; Khanchuk et al., 1997) have associated porphyry Cu-Au mineralization (Khanchuk, 2000). The Late Cretaceous (Early-Late Cretaceous; 114-95 Ma) granodiorite-granite plutons are accompanied by W-Sn mineralization, and the Late Cretaceous-Paleogene (73-53 Ma) Li-F leucogranitic suites are accompanied by W-Sn-Be-Ta mineralization (e.g., Tigrinoe, Zabytoe deposits; Rub et al., 1982) (Fig. 1). Together, different aged W deposits reflect the evolution of W-bearing orogenic granitoid magmatism of the Central Sikhote-

Alin (Soloviev, 1997, 2008). Subduction re-commenced in the Late Cretaceous-Paleogene in the Eastern Sikhote-Alin led to the formation of Sn-base metal deposits with similarities to Bolivian Sn deposits (Gonevchuk et al., 2010).

The Central Sikhote-Alin orogenic belt also contains Au (typically with minor W) deposits, some of which exceed 100t of contained gold (e.g., Stepanov et al., 2013) (Fig. 1). The Glukhoe, Blagodatnoe, and especially Malinovskoe Au deposits are the most significant; some of them are found in close proximity with skarn and stockwork scheelite deposits such as Kordonnoe, Skrytoe etc. These Au deposits are characterized by a distinct Au-As-Bi-W signature, common scheelite, arsenopyrite, and pyrrhotite in Au-bearing zones of silicification and sericitization, intense quartz veining and stockwork. These deposit characteristics, and association with shallow eroded Early Cretaceous ilmenite-series monzodiorite-granodiorite-granite plutons, fit the reduced intrusion-related Au deposit model defined by Thompson et al. (1999), Lang and Baker (2001), Hart (2007). Correspondingly, genetic links of the reduced-type W and Au deposits in the Central Sikhote-Alin associated with the Early Cretaceous ilmenite-series plutonic suites have been suggested (Soloviev and Krivoschekov, 2011).

3. District Geology

The Lermontovskoe deposit is part of a 20x15 km mineralized district that includes numerous W-base metal (e.g., Olympyiskoe, Oshaninskoe, Svetloe, Rubezhnoe) and Au (Au-W) occurrences and Au placers (Fig. 2). Other mineralized clusters of the Central Sikhote-Alin Au-W-Sn metallogenic belt are mostly aligned with the Central Sikhote-Alin Fault, but the Lermontovskoe cluster follows a northeast-trending fault zone splaying off the Central Sikhote-Alin Fault. The splay structure is interpreted as a northwest-dipping thrust-fault zone some 3-4 km wide (e.g., Gvozdev, 2006). The area is part of a Late Jurassic-Early Cretaceous accretion prism (Samarka terrane, after Khanchuk, 2000) and is composed of tectonically piled and locally overthrusted sheets (slices) of fine-clastic Jurassic turbidites alternating with tectonic melange units, oceanic basalts, and units of oceanic cherts and turbidites. The turbidites have local slump structures and graded bedding and possibly formed on the slope of a submarine trough. They contain fragments of oceanic crust such as Devonian ophiolites, Upper Paleozoic and Triassic cherts, and Upper Paleozoic limestones and basalts (Izosov et al., 1988; Khanchuk, 2000). A series of northeast-trending faults divide the

terrain into a number of elongated domains. The Samarka Terrane is bordered to the east by the turbidite-dominant Early Cretaceous terrane.

The mineralized district incorporates series of variously-sized plutons and dikes of mafic to intermediate and granitic rocks representing the Jurassic, Early Cretaceous, and Late Cretaceous (Early-Late Cretaceous) plutonic suites (Fig. 2). Similar to the other mineralized districts of the Central Sikhote-Alin (e.g., Soloviev and Krivoschekov, 2011; Jahn et al., 2015; Soloviev and Kryazhev, 2017), the W-Au-base metal and Au(±W) mineralization in the district is related to the Early Cretaceous multiphase monzodiorite-K-granodiorite-granite plutonic suite formed shortly after the accretionary tectonics ceased (e.g., Sato et al., 2006).

4. Igneous Rocks

Three plutonic to subvolcanic suites are distinguished in the deposit area. Oldest are Middle to Late Jurassic (Gvozdev, 2007a) basalts, gabbro and pyroxenite dikes, sills, and flows. The sills are widespread and alternate with metasedimentary rocks over many hundreds of metres.

The Early Cretaceous granodiorite to granite Vasilievsky suite comprises variously-sized plutons (Shivkinsky, Gorbunsky and other), smaller stocks including the Lermontovskoe stock, and mafic (?) to intermediate and felsic dikes. These granitoid rocks have been initially dated by the Rb-Sr method at 127±4.5 Ma (Shivkinsky pluton) to 124-126±8 Ma (Lermontovskoe stock), with the initial $^{87}Sr/^{86}Sr$ ratios being from 0.70975 to 0.70946, respectively (Rub et al., 1982; Khetchikov et al., 1998). This is similar to the age (122.7-122.9 Ma, with $^{87}Sr/^{86}Sr$ = 0.7088 to 0.07089) of the quartz-scheelite mineralization at the Lermontovskoe deposit (Khetchikov et al., 1998; Gvozdev, 2007a); consistently, the Vasilievsky suite is thought to be parental for the W skarn deposits in the district (Rub et al., 1982; Kovalenko et al., 1988; Sato et al., 2006). However, a different (much younger - 105.6±2.1 Ma) age of the Shivkinsky pluton was later obtained by the zircon U-Pb method that appears to be more reliable (Sakhno et al., 2012). It is similar to the age of granitoid intrusions (from 104±1.3 Ma to 103±1.5 Ma, by the zircon U-Pb method; Sakhno et al., 2012) and mineralization (100-102±1 Ma, by Rb-Sr method; Khetchikov et al., 1999) of the skarn W-Au-base metal Vostok-2 deposit, thus suggesting a uniform age of this mineralization in the Central Sikhote-Alin (Sakhno et al., 2012).

Youngest is the Late Cretaceous (Early-Late Cretaceous) Samuro-Bikinsky plutonic suite comprising large granitoid plutons and smaller stocks of gabbro, diorite, monzodiorite, granodiorite, and granite as well as numerous mafic (andesite to andesite-basalt) dikes. Their radiometric age was reported at 108-64 Ma (by K-Ar and Rb-Sr methods) and they are associated with W-Sn mineralization (e.g., Kovalenko et al., 1988).

The small (2.5 km^2) equant Lermontovskoe stock (Fig. 3) is satellitic to the larger Shivkinsky pluton, has shallow-dipping (25-40^o) roof contacts that steep to 55-85^o to a depth and has numerous apophyses extending up to 100 m away from the intrusive margin. The stock is composed of medium-grained biotite granodiorite, with mafic (monzodiorite) xenoliths or enclaves and locally (in the endocontacts) evolving to monzonite and tonalite, and younger phases of biotite granite and leucogranite-aplite (Table 1) forming smaller stocks and dikes cutting granodiorite; larger granitic bodies encountered by drilling at deeper levels of the Lermontovskoe stock. Granodiorite and granite contain biotite, with rare amphibole (0-3 vol.%) in the granodiorite. According to Kovalenko et al. (1988), biotite in the granodiorite has high magnesium (7.7-10.1 wt.% MgO), titanium (3.1-5.4 wt.% TiO_2), and alumina (12.8-19.9 wt.% Al_2O_3), and low Fe_2O_3 (<0.9 wt.%). Accessory minerals include ilmenite, apatite, zircon, monazite, rutile, scheelite, garnet (containing 15-20 mol.% pyrope, 67-74 mol.% almandine, and up to 10 mol.% spessartine) and cordierite (Table 1; Rub et al., 1982; Kovalenko et al., 1988). Accessory apatite contains 1.9-3.9 wt.% F and up to 0.8 wt.% Cl; tungsten content in this apatite is high (80-90 ppm W; Kovalenko et al., 1988). Numerous mafic (monzogabbro-porphyry, locally identified also as “lamprophyre”) dikes crosscut the Early Cretaceous granitoid rocks.

On the total alkalis vs. SiO_2 diagram (Fig. 4A), the rocks assigned to the Early Cretaceous plutonic suite lie in the upper part of the calc-alkaline field, marginal to the midalkaline field, as defined by Middlemost (1997). Owing to their elevated K_2O (K_2O/Na_2O >1) content, the rocks belong to the high-K calc-alkaline series (Table 2; Fig. 4B). They are also peraluminous (Fig. 4C). The rocks have Fe_2O_3/FeO< 0.4, which, together with the dominance of ilmenite and minor rutile and titanite, indicates reduced (ilmenite-series, after Ishihara, 1981) to weakly-oxidized intrusions. On a Rb-(Y+Nb) discrimination diagram, samples plot in the post-collisional granite field (Fig. 4D). In addition to high K, the rocks have elevated Mg, Ti, P, F, Co, Ni, V, Ba, and Sr contents, with moderate Rb and low Li, Be, Nb, Mo, and Sn contents (Table 2), as compared to the Late Cretaceous (Early-Late Cretaceous) granitoids accompanied by W-Sn mineralization

(Rub et al., 1982; Kovalenko et al., 1988; Gvozdev, 2006, 2007a). The granodiorite is characterized by LREE-enrichment (La_N/Yb_N = 10-12) and lack of to weak Eu anomaly (Table 3).

5. Deposit Geology

The deposit area is underlain by a Jurassic-Lower Cretaceous turbidite sequence containing lenses and sheets of chert (quartzite), carbonate rocks, and mafic volcanic rocks (Figs. 2, 3). They have been intruded by stocks of the Early Cretaceous plutonic suite including the Lermontovskoe stock. Close to the stock contacts, sedimentary rocks have been converted to calcite (with dolomite admixture ?) marble, biotite ±amphibole ±cordierite hornfels, and quartzite, with subsequent development of skarns and post-skarn alteration assemblages in a narrower zone of the stock endo-exocontact. The complex contact shape of the stock (numerous apophyses), coupled with numerous late intrusions and a structural overprint, have further complicated the shape of the orebodies. Skarns are best developed in marble units; some thin-bedded chert/marble/hornfels units are also overprinted by skarn.

Mineralization is hosted by separate bodies of skarn in roof pendants of the Lermontovskoe stock (Figs. 3, 5). These skarn bodies vary in shape (from lens-like to pillar-shaped), lateral extent (from 25 m to 640 m), thickness (from 1m to 80 m), internal structure (from massive lodes to stockworks), composition (from skarn to zones of phyllic alteration after skarns), and W content (from 0.1% to 15-30% WO_3). Mineralization extends 80-120 m from surface (Fig. 6). There are 23 orebodies in total delineated over the deposit area, but most resources are contained in the eight largest bodies (Belyansky et al., 2011).

The orebodies have a distinct mineral zonation from phyllic alteration most proximal to granodiorite (and partially overprinting it) and containing the most W, through a zone of hydrosilicate (amphibole-dominated propylitic) alteration overprinting skarns and containing the most sulfides with significant scheelite, to a distal zone of retrograde and prograde skarn (with relicts of marble, hornfels, and quartzite) with lesser sulfide and scheelite, and finally unaltered metasedimentary rocks (Fig. 6). The zonation reflects a progression from prograde skarn through mineralized retrograde skarn and hydrosilicate alteration to phyllic alteration, where each stage partially overprints its predecessor. The main W-sulfide orebodies are where retrograde skarn is overprinting by mineralized zones of hydrosilicate and phyllic alteration (locally in excess of 10% WO_3 in zones of phyllic alteration; Fig. 5). Phyllic alteration is also developed beyond the skarn

orebodies, in metasedimentary rocks and especially in the Lermontovskoe stock; this expands the overall mineralized contour, although with much lower grades typically not exceeding 0.5-0.7% WO_3. The development of phyllic alteration outside skarn contours "seals" separated (e.g., disconnected by intra-mineralization intrusions) skarn zones into more continuous mineralized packages.

6. Hydrothermal Assemblages and Mineralization

Hydrothermal mineral assemblages at Lermontovskoe include prograde calcic skarn, retrograde skarn, hydrosilicate (propylitic) alteration, and phyllic alteration (Figs. 7, 8). Prograde and retrograde skarns are intersected by granodiorite of the Lermontovskoe stock, whereas hydrosilicate (propylitic) alteration overprints the granodiorite. Phyllic alteration overprints both granodiorite and granite/leucogranite of the Lermontovskoe stock. All alteration assemblages are cut by the late mafic dikes.

6.1 Prograde and retrograde skarns

Prograde skarn mineralogy and zonation are obliterated by later alteration except in the outer parts of mineralized zones most distal from the granodiorite contact(s). Here, zones of massive green to dark-green fine-grained pyroxene (diopside-hedenbergite, with 68-70 mol.% hedenbergite; Table 4) lie along marble-hornfels contacts, with locally abundant calcite and/or idocrase (up to 20 vol.% each). Wollastonite locally rims pyroxene skarn in marble, and very minor brown to reddish-brown garnet (grossular-andradite, with ~33-39 mol.% andradite; Table 4) may be developed between pyroxene and wollastonite zones, or rim the pyroxene zone, if wollastonite is absent (Fig. 8). Pyroxene to pyroxene-plagioclase (labradorite-bitovnite with 70-80 mol.% anorthite) skarns fully replacing smaller hornfels lenses in marble are also present. In addition, irregular branching veinlets of pyroxene rimmed by wollastonite are also developed in marble.

Retrograde skarn assemblages are typically limited to former prograde skarn bodies. Their weakest development is marked by quartz that has partially replaced prograde skarn minerals, but may progress to pervasive or vein-like replacement by quartz with re-crystallized pyroxene ±garnet (Figs. 8, 9). Retrograde skarn pyroxene is dark-green, is distinctly associated with quartz, and is much more ferroan than prograde skarn pyroxene (86-90% mol.% hedenbergite and 6-8 mol.% johannsenite). Rare brownish-red to red garnet contains 9-17 mol.% andradite and 21-28 mol.% spessartine+almandine (Table 4). The retrograde character

of this skarn is supported by minor but ubiquitous amphibole (ferroactinolite; Table 4) that replaces prograde skarn pyroxene and is associated with quartz and minor calcite. Sulfides (mostly pyrrhotite, minor chalcopyrite) and scheelite are present, but typically <5 vol.% in total (Fig. 9). Scheelite has pale yellow luminescence and low Mo content (0.05-0.5 wt.% MoO_3; Kudrin et al., 1979). The grade in the retrograde skarn is typically less than 0.5 wt.% WO_3.

The development of late (mostly phyllic) alteration assemblages along the granodiorite contact(s) commonly obscures the skarn-granodiorite relationships, but where late alterations is less intense, it appears that skarns are cut by granodiorite. Notably also no skarn (endoskarn) development over granodiorite is observed; instead, it appears that the skarns were developed entirely over the host metasedimentary rocks. All relict lithologies in skarn zones are metasedimentary, and skarn zonation is linked to marble-hornfels contact(s) suggesting that skarns predate granodiorite intrusion.

6.2 Hydrosilicate (propylitic) alteration

Hydrosilicate (propylitic) alteration assemblages overprinting prograde and retrograde skarns include pyroxene-free quartz-amphibole, locally biotite-amphibole-quartz, and amphibole-chlorite-quartz assemblages (Figs. 8, 9). Pyrrhotite is abundant, forming massive aggregates, with minor chalcopyrite. Minor minerals include calcite, chlorite, plagioclase, and titanite. There is a distinct zonation of hydrosilicate (propylitic) alteration overprinting skarns: the replacement starts with the development of amphibole-quartz aggregate (with minor chlorite, calcite, and pyrrhotite) replacing skarn pyroxene, further advances with the development of abundant pyrrhotite-quartz (with subordinated amphibole) aggregate, and culminates with the development of quartz-dominated aggregate (with minor amphibole, pyrrhotite, and chalcopyrite). Amphibole is represented by a low-Fe variety (actinolite; Table 4) as compared to the retrograde skarn amphibole. Biotite and/or phlogopite are locally present in the outermost hydrosilicate alteration zones, especially beyond skarn bodies, where it affects hornfels. Scheelite is ubiquitous and especially abundant in association with amphibole and sulfides. It has white luminescence and a low Mo content (0.01–0.05 wt.% MoO_3; Kudrin et al., 1979). Retrograde skarn overprinted by hydrosilicate alteration typically contains 1-2 wt.% WO_3.

A very specific plagioclase-rich (with minor titanite, phlogopite, amphibole, and chlorite) assemblages is locally developed, where hydrosilicate alteration overprints aluminosilicate rocks (granodiorite etc.). Plagioclase is high-calcic (from An_{70-90} to An_{50-70}; Gvozdev, 2007b). The zonation evolving from plagioclase-dominated to plagioclase-quartz-biotite (phlogopite) and then to plagioclase-pyrrhotite-quartz and amphibole-pyrrhotite-quartz assemblages (cf. Gvozdev, 2007b) indicates the development of hydrosilicate (propylitic) alteration. This assemblage also contains scheelite, locally in high abundance (Fig. 9).

6.3 Quartz-sericite(muscovite)-carbonate-sulfide (phyllic) alteration

The deposit is characterized by intense development of quartz-sericite (muscovite)-carbonate assemblages, locally containing also biotite (phlogopite), chlorite, plagioclase, abundant apatite, and trace tourmaline. These zones of phyllic alteration have the highest W grade and variable amounts of Cu, Zn, Pb, As sulfides and sulfosalts as well as native Bi and Au. These alteration assemblages overprint the Lermontovskoe granodiorite stock, granite and leucogranite-aplite dikes, prograde and retrograde skarns, zones of hydrosilicate alteration and, to a lesser extent, metasedimentary (mostly silicic) rocks. Two phyllic alteration assemblages are recognized.

An early assemblage comprises coarse-grained quartz-muscovite (locally, in outer zones – quartz-phlogopite), minor carbonate (including Fe-carbonate), albite, and most abundant apatite and scheelite. It forms anastomosing veinlets that merge into zones of pervasive replacement (especially in the granodiorite) (Fig. 8). The alteration starts with the development of dark micas (overprinting Fe-rich protoliths - pyrrhotite- and/or biotite-rich hydrosilicate alteration zones, pyroxene-pyrrhotite retrograde skarn, and biotite hornfels), albite, and quartz. It progresses through dominantly muscovite-quartz aggregates, with subordinated carbonates (calcite, ankerite, siderite), and albite, to almost monomineralic quartz, the latter forming the central core of the alteration zones. Arsenopyrite is the dominating sulfide mineral, and is most abundant in the outer zone containing dark micas, where it locally forms small monomineralic lenses. Scheelite and apatite (fluorapatite to fluorcarbonate-apatite; Rub et al., 1982) are abundant and locally form large-crystalline aggregates (Figs. 8, 9).

Late phyllic alteration assemblage comprises fine-grained quartz-sericite-carbonate, with minor chlorite, albite, apatite, scheelite, and minor pyrrhotite, chalcopyrite, sphalerite, galena, various sulfosalts and

tellurides, and Bi and Au minerals. Chlorite replaces dark micas, whereas albite is formed in expense of Ca-plagioclase. Early and late phyllic alteration zones are commonly transitional, where late alteration forms a patchy to pervasive overprint or thin sheeted veins. Late phyllic alteration is zoned from outer chlorite-carbonate-albite, with minor sericite, through sericite-quartz to quartz-dominant core. Sulfides are finely disseminated throughout and also form larger aggregates in the innermost (quartz) zone. Sulfide content is typically low (<5-10 vol.%), except where phyllic alteration overprints skarns with abundant sulfides.

Scheelite is abundant in phyllic alteration assemblages (locally up to 30 vol.%), and the WO_3 grade in skarns overprinted by hydrosilicate and then phyllic alteration is high (locally >10 wt.% WO_3). Two generations of scheelite are recognized corresponding to early and late phyllic alteration. Early scheelite is associated with most abundant early arsenopyrite, has white-blue luminescence and contains low Mo (0.005-0.01 wt.% MoO_3; Kudrin et al., 1979). Late scheelite is associated with chalcopyrite and pyrrhotite, has blue luminescence, contains trace to no Mo (<0.001-0.005 wt.% MoO_3; Kudrin et al., 1979), and is enriched in Eu (Table 5). Trace wolframite (ferberite; Rub et al., 1982) post-dates scheelite and is associated with sphalerite. Sphalerite replaces pyrrhotite, early arsenopyrite, and chalcopyrite but contains pyrrhotite, chalcopyrite, and stannite emulsions.

Phyllic alteration assemblages also contain minor Bi and Au mineralization (Fig. 10). Native Bi and bismuthinite are associated with chalcopyrite, pyrrhotite and scheelite, whereas lesser Bi-tellurides (e.g., hedleyite) and Bi-Pb-Sb sulfosalts (e.g., kosalite, galenobismuthite) are associated with sphalerite and galena (Stepanov and Gvozdev, 1987; Gvozdev, 2007a). Native Au (fineness 850‰) is associated mostly with a chalcopyrite and native Bi-bismuthinite assemblage (Stepanov and Gvozdev, 1987). Native Au forms microinclusions in chalcopyrite, partly replaces arsenopyrite, and also forms larger isolated grains in quartz and other gangue minerals (Fig. 10). A late assemblage of Ag-Pb-Sb sulfosalts containing Ag-tetrahedrite, freibergite, jemsonite, meneginite, miargyrite, and pirargyrite is associated mostly with galena and post-dates the tellluride-Pb-Sb-Bi-sulfosalt assemblage (Gvozdev, 2007a).

7. **Fluid Inclusion and Stable Isotope Study**

Kokorin and Kokorina (1977) identified various types of liquid-gaseous to gaseous-liquid fluid inclusions mostly in minerals from phyllic alteration assemblages. Inclusions homogenized into either

gaseous or liquid phase over a wide range of temperatures (~450 to <150°C); CO_2 was the only carbonic species reported in some inclusions. Multiphase fluid inclusions containing halite homogenized either by halite dissolution, or by vapor bubble disappearance. Khetchikov et al. (1998) reported high-salinity (>30 wt.% NaCl-equiv.) fluid inclusions in quartz-scheelite assemblages, as well as inclusions with CO_2. Stable isotope study by Sakhno et al. (2012) yielded the $\delta^{18}O$ values of +11.1‰ for magmatic quartz from the Shivkinsky pluton. Gvozdev et al. (1999) reported $\delta^{18}O$ values of +9.0 to +13.0‰ and $\delta^{13}C$ values of -5.6 to -3.9‰ for carbonates from altered skarns, $\delta^{18}O$ values of +14.2 to +16.5‰ and $\delta^{13}C$ values of -11.0 to -5.0‰ for carbonates from late carbonate and carbonate-sulfide veinlets, and $\delta^{34}S$ values of -6.7 to -4.0‰ for sulfides from various mineral assemblages (Gvozdev, 2007a).

The present fluid inclusion study is predicated on the mineral paragenesis sequence described above (Fig. 11; Table 6). Consistently, fluid inclusions were studied in minerals from prograde and retrograde skarn, hydrosilicate and phyllic alteration assemblages. Samples for this study are from an open pit excavated at the Central mineralized zone of the deposit.

Thirty-two doubly polished sections of 0.3 to 0.5 mm thick were prepared from 22 samples for fluid inclusion petrography and microthermometry. Microthermometric analyses were made using the UMTK-3 freezing–heating stage designed by VIMS Institute and modified by TsNIGRI Institute, Russian Geological Survey, to allow low-temperature experiments. Cooling is by liquid N_2 flow. The stage uses a chromel-alumel thermocouple that can range from below −180 to over +650 °C. The stage was periodically calibrated using the boiling temperature of pure N_2 (−196 °C), triple point for pure CO_2 (−56.6 °C), temperatures of ice melting in standard NaCl solutions (from −18° to −1°C), melting temperatures of $AgNO_3$ (210°C), K_2CrO_7 (398°C), and NaI (651°C). Final ice-melting temperatures are accurate to ±0.2°C, clathrate melting temperatures to ±0.5°C, eutectic temperatures to ±1.5°C, and homogenization temperatures to ±5°C. Heating rate (at above 30°C) was 5°C/min up to a heating limit of 650°C.

The fluid inclusion study targeted fluid inclusion assemblages (FIA), i.e., closely associated groups or trails of fluid inclusions with visually similar phase ratios and similar shapes (Goldstein and Reynolds, 1994). The sequence of entrapment can be inferred from observations of rare primary inclusions distributed randomly away from fractures, crosscutting trails of FIA along individual fractures or pseudosecondary trails

that are associated with healed microfractures terminated by crystal growth zones (Roedder, 1984). Groups of fluid inclusions are linked to various mineralizing stages on the basis of their absence in younger mineral assemblages (Masterman et al., 2005). Accurate discrimination of different FIAs is critical for correctly interpreting fluid inclusion data (Goldstein and Reynolds, 1994).

For the gas chromatography analysis, 1-gram quartz separates were prepared by magnetic separation and handpicking under a binocular microscope. Mineral separates were crushed in an agate mortar to 0.25-0.5 mm, followed by sample cleaning in a HNO_3 aqueous (1:1) solution (e.g., Bottrell et al., 1988) and water-flow electrolytic cleaning in an ultrasound bath for 3 hours. Samples were then dried and put into a quartz glass reactor vacuumed at 110^{o}C and filled with helium. Fluid inclusions were liberated by heating to 500^{o}C and maintaining that temperature for 15 minutes. The gases extracted were introduced into a gas chromatograph equipped with a gas flow divider to allow simultaneous determination of H_2O, CO_2, and CH_4. Then, the heated samples were leached with de-ionized water in an ultrasound bath for 15 minutes. The leachate solution was separated by centrifuging and then analyzed by ICP-MS (Elan-6100) for cations (Na^+, K^+, Ca^{2+}, Mg^{2+}) and by ion chromatography for anions (Cl^-, F^-, SO_4^{2-}, HCO_3^-, B^{3-}). The concentration of HCO_3^- was calculated using the cation/anion balance and all concentrations were normalized to the water content.

Sulfides for the isotopic study were extracted by a dental drill and/or by the hand picking of chips. Sulfide powders were analyzed by conventional methods using the techniques of Robinson and Kusakabe (1975). Sulfides were decomposed by reaction with CuO at 750^{o}C, and isotope ratios were measured from SO_2 on a MI-1201 mass spectrometer. An analytical uncertainty of $\pm$0.2‰ (2 σ) for $\delta^{34}S$ was estimated from internal standards of homogenous pyrite from the Gaiskoe deposit in the Southern Ural ($\delta^{34}S_{VCDT}$=+0.7‰).

7.1 Fluid inclusions in garnet and pyroxene from prograde and retrograde skarns

Rare primary fluid inclusions in garnet and pyroxene are represented by multiphase (multisolid) inclusions (type 1A and 1B) that typically occur as isolated individual inclusions (Fig. 11A-D; Table 6). Type 1A inclusions in core zones of garnet crystals are tentatively assigned to the prograde skarn stage and contain 3-5 anisotropic colorless (to semi-transparent white) and black opaque solid phases together occupying up to

85 vol.%, and a small (15-20 vol.%) gas bubble. No halite or sylvite was identified. Large re-crystallized pyroxene (hedenbergite) crystals are associated with quartz and pyrrhotite in the retrograde skarn and contain type 1B inclusions with 20-40 vol.% halite, 2-3 anisotropic colorless (to semi-transparent white) and black opaque solid phases, and 30-60 vol.% gas. The solid phases other than halite are not interpreted as daughter minerals (Roedder, 1984).

On heating, type 1A inclusions exhibit disappearance of a gas bubble at 350-390°C and then decrepitation at 500-530°C, with no dissolution of the solid phases. In type 1B inclusions, gas bubble disappears at 310-350°C and halite dissolves at 450-500°C (Table 6; Fig. 12). Further heating leads to decrepitation of these inclusions at 550-560°C, with no dissolution of the other solid phases.

Gas bubble homogenization temperatures (350-390°C) for type 1A inclusions are significantly lower than typical temperatures of prograde skarn formation (~550-650°C; e.g., Einaudi et al., 1981; Meinert et al., 2003, 2005), suggesting that measured gas bubble homogenization temperatures are significantly lower than actual fluid inclusion entrapment temperatures. Such difference can be estimated for 1B type inclusions also exhibiting low gas bubble homogenization temperatures (310-350°C), as halite dissolution at 450-500°C allows salinity estimates in the NaCl-H_2O system (Bodnar and Vityk, 1994) and indicates high salinity of 53 to 60 wt.% NaCl-equiv. (Table 6). Minimum pressure can also be estimated for the 1B inclusions using vapor bubble homogenization and halite dissolution temperatures (e.g., Roedder, 1984). Using the isochores of a 50-60 wt.% NaCl solution (Atkinson, 2002; Becker et al., 2008), this yields minimum pressure estimates of ~1400-1500 bars (Fig. 12), with temperature correction of 140-150°C. Therefore, similar, or even greater, temperature corrections are necessary to estimate entrapment temperatures for type 1A inclusions. Pressures of 1400-1500 bars correspond to depths of 5.4-5.8 km, assuming lithostatic conditions (cf. Fournier, 1999), which is consistent with weakly porphyritic features and the inferred lower hypabissal level of the Lermontovskoe stock.

7.2 Fluid inclusions in quartz and scheelite from hydrosilicate (propylitic) alteration

Primary and pseudosecondary fluid inclusions (type 2 inclusions, or FIA) typically form variably-sized clusters and short trails. Type 2 inclusions can be subdivided into coexisting type 2A inclusions with >95 vol.% gas, and aqueous liquid-gaseous type 2B inclusions with 30-40 vol.% gas (Fig. 11E-I; Table 6). These

inclusions contain a carbonic phase including significant methane as evidenced by clathrate final melting temperatures in the range of +14.5 to +15.5°C (Burruss, 1981). Carbonic phases in type 2A inclusions homogenize at -88.0 to -90.0°C into liquid, allowing estimation of CH_4 mole fraction at >99 mol.% (CO_2:CH_4=<0.01) (Thiery et al., 1994) (Table 6). Final homogenization of the type 2B inclusions occurs at 360-380°C into liquid.

Assuming contemporaneous entrapment of coexisting type 2A and 2B inclusions under two phase immiscibility (boiling), the trapping pressures of these fluid inclusions can be established using trapping temperatures (360-380°C) for the high-density type 2B fluid inclusions and densities for the low-density type 2A fluid inclusions (e.g., Roedder, 1984). On this basis and using the computing programs of Bakker (2003), the estimation of the trapping pressure yields the values of 1300 to 1400 bars. Due to the fluid boiling, no pressure correction is necessary for the homogenization temperature of 360-380°C. Pressures of 1300 to 1400 bars correspond to depths of 5.0-5.5 km, assuming lithostatic conditions (cf. Fournier, 1999).

7.3 Fluid inclusions in quartz, carbonate and scheelite from the early (quartz-muscovite-carbonate-apatite-arsenopyrite-scheelite) assemblage of phyllic alteration

Primary and pseudosecondary multiphase type 3 inclusions are hosted by quartz and carbonate as isolated individual inclusions and as clusters. They contain 2-6 solid phases including a typically large (30-40 vol.%) halite cubes, and a small (10-20 vol.%) gas bubble (Fig. 11J-M). Gas bubbles disappear at 250-290°C and halite dissolves at 350-400°C (Table 6; Fig. 12). The other solid phases remain undissolved at 650°C (limit of heating). Salinity estimates in the NaCl-H_2O system (Bodnar and Vityk, 1994) are 42 to 47 wt.% NaCl-equiv. (Table 6). Minimum pressure estimates for the type 3 inclusions, using temperatures of gas bubble disappearance and halite dissolution (e.g., Roedder, 1984), and the isochores for a 40-50 wt.% NaCl solution (Becker et al., 2008), are ~1000-1100 bars (Fig. 12), with 100-110°C temperature corrections required. Such pressures are consistent with those estimated above for the other fluid inclusion types; however, the upper limit of the corrected temperatures (~450-460°C) appears to be too high for this mineral assemblage. Consequently, this may reflect limitations of the method used (Roedder, 1984; Becker et al., 2008), given that $CaCl_2$, $MgCl_2$ and other salts will affect halite solubility (Crawford, 1981).

Primary and pseudosecondary type 4 fluid inclusions (or FIA) are numerous in quartz, scheelite, and carbonate as variably-sized clusters and short trails alongside type 3 inclusions. Their timing relative to type 3 inclusions is unclear. Type 4 inclusions are represented by coexisting gaseous type 4A inclusions containing 80-90 vol.% gas, and aqueous liquid-gaseous type 4B inclusions containing 40-50 vol.% gas (Fig. 11N-O). Type 4A inclusions contain a carbonic phase including significant methane that is evidenced by clathrate final melting temperatures of +10.5 to +11.5°C (Burruss, 1981). Carbonic phases in type 4A inclusions homogenize into gas at -83 to -85°C leading to an estimated CH_4 mole fraction of >99 mol.% (CO_2:CH_4=<0.01) (Thiery et al., 1994) (Table 6). Final homogenization of type 4A inclusions occurs at 390-420°C into gas. Type 4B inclusions have eutectic first melting temperature of -25°C suggesting dominant NaCl in solution (Crawford et al., 1981). Final ice melting temperature of -6.5 to -6.0°C indicates salinities of 9 to 10 wt.% NaCl-equiv. (Bodnar and Vityk, 1994) (Table 6). Final homogenization of the type 4B inclusions occurs at 390-420°C into liquid.

Assuming contemporaneous entrapment of the coexisting type 4A and 4B inclusions under two phase immiscibility (boiling), the trapping pressures for these fluid inclusions can be established using trapping temperatures (390-420°C) for the high-density type 4B inclusions and densities for the low-density type 4A inclusions (e.g., Roedder, 1984). As above, trapping pressures of 1150 to 1200 bars have been estimated. Due to the fluid boiling, no pressure correction is necessary for the homogenization temperature of 390-420°C.

7.4 Fluid inclusions in quartz from the late (quartz-sericite-carbonate-sulfide-Bi-Au) assemblage of phyllic alteration

Primary and pseudosecondary type 5 fluid inclusions (or FIA) form variably-sized clusters and short trails in quartz, and include essentially gaseous type 5A inclusions with 70-80 vol.% gas, and aqueous liquid-gaseous type 5B inclusions containing 15-25 vol.% gas (Fig. 11Q-R). These inclusions contain a carbonic phase including significant methane that is evidenced by clathrate final melting temperatures of +11.7 to +12.0°C (Burruss, 1981). Type 5A inclusions have final CO_2 melting temperature of -67.0 to -64.5°C, indicating a CH_4 mole fraction of about 0.9 (CO_2:CH_4=10:90) (Thiery et al., 1994) (Table 6). Final homogenization of type 5A inclusions occurs at 340-360°C into gas. The type 5B inclusions have eutectic first melting temperature of -26.0 to -24.2°C suggesting dominant NaCl in solution (Crawford et al., 1981).

Final ice melting temperature of -8.2 to -6.2°C indicate salinities of 9.5 to 12 wt.% NaCl-equiv. (Bodnar and Vityk, 1994) (Table 6). Final homogenization of type 5B inclusions occurs at 340-360°C into liquid.

Again, assuming contemporaneous entrapment of the coexisting type 5A and 5B inclusions under two phase immiscibility (boiling) and using the same method as above, trapping pressures of 370 to 400 bars have been estimated. Due to the fluid boiling, no pressure correction is necessary for the homogenization temperature estimate of 340-360°C.

Another "pair" of primary and pseudosecondary type 6 fluid inclusions (or FIA) studied in quartz is quite rare, occurs mostly in small clusters and short trails, and includes coexisting essentially gaseous type 6A inclusions containing >95 vol.% gas, and multiphase type 6B inclusions with halite (20-25 vol.%) and gas (20-25 vol.%) (Fig. 11S-U). Type 6A inclusions have final CO_2 melting temperature of -63.5°C, and carbonic phase homogenization temperatures of -12.0 to -18.0°C, leading to an estimated CH_4 mole fraction of about 0.5 (CO_2:CH_4=50:50) (Thiery et al., 1994) (Table 6). In type 6B inclusions, halite dissolves at 200-230°C and gas homogenizes at 250-300°C. Salinity estimates in the NaCl-H_2O system (Bodnar and Vityk, 1994) for the type 6B inclusions yielded values of 32-34 wt.% NaCl-equiv. (Table 6).

Assuming contemporaneous entrapment of the coexisting type 6A and 6B inclusions under two phase immiscibility (boiling), and using the same method as above, trapping pressures of 300 to 350 bars have been estimated. Due to the fluid boiling, no pressure correction is necessary for the homogenization temperature of 250-300°C. Notably this temperature range is consistent with the presence of native bismuth in this mineral assemblage ($T_{melting}$ = 271.4°C).

7.5 Bulk fluid geochemistry

Bulk gas chromatography results are affected by secondary inclusions and must be treated with caution. Nevertheless, results (Table 7) show elevated concentrations of Mg, Na and Ca for hydrosilicate stage samples, with concentration of Mg exceeding those of Na and Ca, whereas Na is dominant for phyllic alteration samples, with lesser Ca. Methane and CO_2 are important in the fluids forming the hydrosilicate assemblage, but the amount of methane is lower for phyllic alteration samples, consistent with microscopic observations. Fluids trapped during formation of the hydrosilicate stage minerals have consistently low CO_2/CH_4 ratios indicating reduced conditions compared to those of phyllic alteration (Table 7).

7.6 Sulfur isotopes

Sulfur isotope values in sulfides from the hydrosilicate ($\delta^{34}S$ = -7.5 to -6.0 ‰) and phyllic ($\delta^{34}S$ = -5.6 to -4.4 ‰) alteration assemblages (Table 8) are distinctly light with a minor but consistent difference between these two alteration assemblages.

8. Discussion

The Lermontovskoe deposit is of special interest because it is a moderately-large and very high-grade W skarn deposit of the reduced type (Einaudi et al., 1981; Kwak and White, 1982). Together with other similar deposits in the Central Sikhote-Alin (e.g., Rub et al., 1982; Gvozdev, 2006, 2007a; Soloviev and Krivoschekov, 2011; Soloviev and Kryazhev, 2017; Soloviev et al., 2017), it is localized in the W-Sn-Au metallogenic belt related to Early and Late Cretaceous ilmenite-series granitoid intrusions that formed in a late- to post-collisional tectonic regime (Khanchuk, 2000). The Lermontovskoe W deposit has low but consistently anomalous gold grades (average 0.23 g/t Au) and elevated As-Bi-Te-Sb indicating that it may be transitional between reduced W skarn and reduced intrusion-related Au+W deposit classes (Thompson et al., 1999; Lang and Baker, 2001; Hart, 2007).

The Lermontovskoe deposit is associated with an Early Cretaceous intrusive of the ilmenite-series high-K peraluminous granitoid rocks (granodiorite to granite). Presence of amphibole, even in trace amounts (< 3 vol.%), indicates the Lermontovskoe stock granodiorite belongs to the I-type; due to peraluminous signatures, the rock can be classified as the peraluminous I-type granitoids (Chappel et al., 2012). According to Chappel et al. (2012), such granitoids can be formed by partial melting of a mafic source rocks; also, although less likely, peraluminous granitic melt can be generated from metaaluminous granite melt by fractional crystallization of amphibole. The Lermontovskoe stock rocks are characterized by elevated Mg, Ti, P, F, Co, Ni, V, Ba, and Sr contents, lack of pronounced Eu-anomaly, well-expressed LREE-enrichment, presence of high-Mg accessory garnet, and high-Ti, high-Mg biotite compositions (Rub et al., 1982; Kovalenko et al., 1988; Soloviev, 1997, 2008; Kruk et al., 2014). These signatures are consistent with an involvement of a deeper, possibly mantle-related magma source. Jahn et al. (2015) suggested that these rocks

were formed due to mantle magma-induced melting of crustal sources, and/or partial melting of sources with significant proportions of mantle-derived material intercalated with older continental crust components in the lower part of the Sikhote-Alin basement, with further crustal assimilation. The links of the igneous rocks at Lermontovskoe with a mantle source, with possible further crust-mantle interaction, are similar to those proposed for the other Early Cretaceous monzodiorite-granodiorite-granite plutonic suites in the Sikhote-Alin accompanied by W-Au-base metal mineralization (Rub et al., 1982; Kovalenko et al., 1988; Soloviev, 1997, 2008; Gvozdev, 2007a). Due to high-potassic character of the rocks, their shoshonitic affinity can be suggested: in late- to post-collisional environment, ilmenite-series high-K to shoshonitic igneous suites (generally of granodiorite composition) can be generated due to mingling of ascending mafic magmas with felsic magmas, the latter generated from the accretionary complex (e.g., Ishihara, 2004; Mair et al., 2006, 2011). This corresponds to possible asthenosphere uplift through a slab window, or asthenosphere mantle ascent caused by lithosphere delamination (Khanchuk, 2000) that, in turn, could have resulted in widespread melting of crustal rocks and emplacement of coeval peraluminous granitic suites in the Early Cretaceous (Kruk et al., 2014).

The ilmenite-dominant, peraluminous and potassic granitoids are typical for reduced W-skarn deposits worldwide, such as the CanTung and MacTung deposits in the Yukon-NWT, Canada, which are related to the Tungsten plutonic suite (Maloof et al., 2001; Hart et al., 2004; Mair et al., 2006, 2011; Rasmussen et al., 2011). However, the peraluminous I-type granitoids at Lermontovskoe are transitional to reduced to weakly-oxidized metaaluminous I-type granitoid suites of reduced intrusion-related Au deposits, such as those related to the Tombstone plutonic suite in the Yukon-NWT, Canada (Maloof et al., 2001; Hart, 2007; Mair et al., 2006, 2011). Genetic links of the igneous rocks at Lermontovskoe to reduced intrusion-related Au deposits are further supported by the plots of the Lermontovskoe igneous rocks in the respective fields of the Fe_2O_3/FeO vs. Rb/Sr diagram (Fig. 13).

The deposit was formed during several hydrothermal stages beginning with prograde and retrograde skarns and followed by hydrosilicate (propylitic) and phyllic alteration assemblages. Petrologic features of the skarn and post-skarn assemblages are consistent with reduced type W skarn deposits (Einaudi et al., 1981; Kwak and White, 1982) thus reflecting the features of the parental ilmenite-series plutonic suite. In particular, pyroxene predominates over garnet in skarns, and is represented by ferrous (hedenbergitic) varieties. The

minor garnet belongs to low-andraditic, grossular-rich (with elevated almandine-spessartine content) variety. No magnetite is present but pyrrhotite is abundant. Low-Mo, high-Eu scheelite also indicates reduced conditions (cf. Soloviev, 1999; Song et al., 2014). Fluid inclusion data further support a reduced environment, as methane is a dominating carbonic species in the fluids at Lermontovskoe, similarly to that at other reduced W skarn deposits (e.g., Mathieson and Clark, 1984; Gerstner et al., 1989).

Hydrothermal stages were alternating with successive intrusion phases (Fig. 7), the latter composing the Lermontovskoe stock and smaller stocks and dikes in its vicinity. In particular, skarns at Lermontovskoe appear to have been formed before emplacement of the granodiorite stock. This suggests older and unexposed intrusions possibly supplied fluids for the skarn formation (cf. Korzhinskii et al., 1984; Shinohara and Hedenquist, 1997; Candela and Piccoli, 2005). Wollastonite forms at temperatures of 650-550^{o}C and pressures exceeding 400 bar in the presence of water-rich, very low-carbonic fluids (X_{CO2}=~0.005, or 0.5 mol.% CO_2) strongly suggesting intrusion-related alteration (Lentz and Suzuki, 2000). The formation of andradite-grossular garnet (10-40 mol.% grossular) in skarns occurs at temperatures of 500-600^{o}C and pressures of 1500-2000 bars under low X_{CO2} (<0.1) (Tailor and Liou, 1978). Pyroxene in skarns is stable at temperatures >450^{o}C (Gustafson, 1974), and this corresponds to the lower temperature limit of the retrograde skarn formation. Fluid inclusion data show that prograde and retrograde skarns at Lermontovskoe were formed at high temperatures (>500^{o}C) and high pressures (1400-1500 bars) from high-salinity (53-60 wt.% NaCl-equiv.) fluids containing no carbonic phases (Table 6; Fig. 14). Fluid inclusions in retrograde skarn assemblages homogenized by halite dissolution suggesting that these high-salinity fluids were exsolved directly from crystallizing magma (Cline and Bodnar, 1994; Bodnar, 1995).

In contrast, hydrosilicate (propylitic) alteration occurred after the emplacement of granodiorite and formed from the highly-carbonic, methane-dominated low-salinity fluids. The fluid inclusion entrapment temperatures (360-380^{o}C) recorded for the type 2 fluid inclusions appear to be too low to establish a direct link to a magmatic melt and may indicate that the fluids were separated at depth and cooled before reaching the mineral deposition level. At this level, even relatively high pressure (~1300-1400 bars) was insufficient to preclude fluid boiling such that the fluids separated into the gaseous (methane-dominated type 1A inclusions) and methane-aqueous (type 1B inclusions) phases. Pressures are lower than those estimated at some other reduced W skarn deposits ranging from 1.7-2.0 kbar to 1.4-2.5 kbar (e.g., Sato, 1980; Guy et al., 1988;

Gerstner et al., 1989); this may indicate overall shallower conditions of the Lermontovskoe deposit formation, consistent with the transition from reduced W skarns to intrusion-related Au deposits.

Hydrosilicate alteration was characterized by very high $a\mathrm{Ca}^{2+}$ resulting in a Ca-plagioclase-quartz-amphibole ±titanite ±biotite) assemblage (cf. Hunt and Kerrick, 1977; Takagi et al., 2007; Rasmussen et al., 2011). Ca-rich fluids are also recorded at other W skarn deposits (e.g., Kwak and Tan, 1981; Santarelli, 1988), and it has been suggested that this Ca-enrichment may reflect partitioning of Ca into magmatic-hydrothermal fluid due to plutonic rock evolution toward those with less calcic plagioclase (cf. Lang et al., 1995; Soloviev, 2015). Also, an involvement of basinal brines is often considered as a possible source of Ca (Barton and Johnson, 2000). Although an influx of basinal brines into the high-temperature, high-pressure core part of hydrothermal deposits has been questioned (Sillitoe, 2010), it appears to be possible at lower temperature and pressure conditions.

Newberry (1983) suggested that Ca in retrograde skarn can be provided due to replacement of prograde skarn garnet by "subcalcic" (almandine- and spessartine-rich) retrograde skarn garnets. This model is plausible at many oxidized and especially redox-intermediate W skarn deposits, with abundant prograde and retrograde skarn garnets. However, application of this model at reduced W skarn deposits, where garnet is a minor mineral strongly yielding to pyroxene in abundance, is limited. In contrast, Ca at retrograde skarn and especially hydrosilicate (propylitic) alteration stages can be liberated by reactions of skarn pyroxene with aqueous-carbonic fluid and its replacement by amphibole (± quartz and calcite), such as

$$\underset{\text{(pyroxene)}}{5Ca(Mg, Fe)Si_2O_6} + 3CO_2 + H_2O = \underset{\text{(amphibole)}}{Ca_2(Mg, Fe)_5(Si_4O_{11})_2(OH)_2} + \underset{\text{(calcite)}}{3CaCO_3} + \underset{\text{(quartz)}}{2SiO_2}.$$

Under lower $a\mathrm{CO}_2$ (e.g., in reduced conditions, and/or under CO_2 removal), Ca can be liberated into the fluid and, under high aW, calcite deposition yields to that of scheelite. An additional role in scheelite deposition can be played by fluid boiling that affects scheelite solubility due to neutralization of acid fluids (Rafal'sky et al. 1984; Wood and Samson 2000). Sulfidation of pyroxene in reduced conditions results in the deposition of pyrrhotite (Burton et al., 1982; Gamble, 1982).

The $\delta^{18}\mathrm{O}_{\mathrm{H2O}}$ values (+9.0 to +13.0‰) obtained for the hydrothermal minerals (Gvozvev et al., 1999) are similar to those (+11.1‰) for magmatic quartz (Sakhno et al., 2012) indicating a magmatic source of water without an incursion of meteoric water. These values also indicate a homogenized mixed mantle-crustal

oxygen source (Faure, 1986). A crustal source of sulfur ($\delta^{34}S$ = -7.5 to -6.0 ‰) can be also suggested (Ohmoto and Goldhaber, 1997; Seal, 2006).

The phyllic alteration stage corresponded to more differentiated magmatic evolution toward most felsic (~74-75 wt.% SiO_2) granite to leucogranite intrusions. Advanced magmatic differentiation promoted enrichment of residual melt in W (Newberry and Swanson, 1986; Newberry, 1998), with Au concentration in the residual felsic melt promoted by the low content of accessory oxides and sulfides and by elevated volatile content (cf. Mustard et al., 2006). The presence of phlogopite is consistent with its higher-temperature (>350^{o}C) stability at reduced (pyrrhotite-stable) conditions. The coarse-grained micaceous (with muscovite and/or phlogopite) rocks are reminiscent of greisens (e.g., Gvozdev, 2007a), however, they lack high-Al minerals (topaz etc.) and high-Li micas required to classify these rocks as "true" greisens typical of many W-Mo, W-Sn, rare metal (Be-Ta-Li) and some other deposits (e.g., Burt, 1981, and references therein; Pirajno, 1992; Stemprok, 1987; Dolejs and Stemprok, 2001). Instead, ubiquitous carbonates (including Fe-carbonate) and plagioclase indicate that these rocks are rather coarse-grained varieties of phyllic alteration (Soloviev and Krivoschekov, 2011). Notably Seedorf et al. (2008) suggested using the term greisen only as a textural modifier for coarse-grained muscovite-quartz aggregates in root zones of porphyry deposits. Similar coarse-grained muscovite-quartz rocks are also reported at some reduced intrusion-related Au deposits (e.g., Kontak and Kyser, 2011).

Fluid inclusions in phyllic alteration minerals suggest a complex process of magma degassing and magmatic-hydrothermal fluid evolution (Fig. 14). Early phyllic alteration was higher-temperature (>450^{o}C) than that of the hydrosilicate alteration stage (360-380^{o}C) indicating a new fluid influx from magma, and the type 3 multiphase fluid inclusions homogenized by halite dissolution indicate the high-salinity (39-50 wt.% NaCl-equiv.), high-pressure (1100-1400 bars) fluid was exsolved directly from crystallizing magma (cf. Cline and Bodnar, 1994; Bodnar, 1995). Later phyllic alteration fluids are low-salinity, methane-dominated carbonic-aqueous fluid was exsolved at slightly lower temperatures (390-420^{o}C) and pressures of 1150-1200 bars. They separated into a gaseous (methane-dominated) (type 4A inclusions) and methane-aqueous (type 4B inclusions) phases (Fig. 14). Further fluid evolution at the phyllic alteration stage occurring at decreasing pressures (370-400 bars to 300-350 bars) and temperatures (340-360^{o}C to 250-300^{o}C) also included boiling episodes causing separation of a gaseous carbonic and saline liquid aqueous phases corresponding to the type

5A and 5B inclusions and the type 6A and 6B inclusions, respectively (Fig. 14), and with increasing CO_2/CH_4 ratio. The significant pressure drop (compared to hydrosilicate and early phyllic alteration) could be related to the pluton unroofing combined with lowering of the brittle-ductile deformation front (Fournier, 1999) corresponding to the magmatic-hydrothermal system collapse, with the formation of deep-penetrating fault and fracture zones. High CO_2 is common in fluids at reduced intrusion-related Au deposits (e.g., McCoy et al., 1997; Baker, 2002; Baker and Lang, 2003) and in late fluids at reduced W skarn deposits (Fonteilles et al., 1989; Gerstner et al., 1989). Baker (2002) linked an abundance of carbonic-rich fluid inclusions to a greater depth of magmatic crystallization, whereas the evolution from CH_4-rich to CO_2-rich fluids can be due to increasing fO_2.

Similarly to the hydrosilicate alteration stage, fluid cooling and especially increasing pH due to boiling and related carbonic phase removal (cf. Drummond and Ohmoto, 1985) were affecting W solubility at the phyllic alteration stage that, together with dissociation of Ca-bearing complexes liberating Ca, promoted massive scheelite deposition (Rafal'sky et al., 1984; Wood and Samson, 2000). The high aCa^{2+} is evident by the presence of high-Ca minerals (apatite, carbonates etc.); Rasmussen et al. (2011) defined similar mineral assemblages as "calcic-sericitic" alteration. Notably no W chloride, fluoride, carbonate complexes, i.e., species commonly associated with high-salinity fluids, are required to form scheelite concentrations, as the role of hydrous W species dominates (Wood and Vlassopoulos, 1989; Wood and Samson, 2000). Probably, a strong role in W transport was also played by phosphate complexes (Manning and Henderson, 1984) evident by the association of scheelite and apatite.

In contrast to W, partitioning of Au in magmatic-hydrothermal process is essentially influenced by the behavior of sulfur, with lower redox conditions promoting sulfide saturation in granitic magmas or facilitating sulfide (bearing Au) precipitation from mineralized fluids (e.g., Lang and Baker, 2001; Yang, 2012). Au transport at low temperatures corresponding to phyllic alteration stage occurs mostly in the form of bisulfide rather than chloride complexes (e.g., Gammons and Williams-Jones, 1997). Close association of Au and Bi also supports their joint transport and precipitation as bisulfide complexes due to reduced conditions and low salinity (low chloride content) of the fluids (e.g., Seward, 1991), or partial scavenging of Au in Bi melt coexisting with the hydrothermal fluid (e.g., Tooth et al., 2008). Gold deposition could have also been

favored by a decreasing Au solubility under a pH decrease that occurred after massive scheelite deposition, the latter favored by fluid boiling and coincident pH increase at the phyllic alteration stage.

The fluid inclusion data indicate early release of high-salinity fluids followed (or accompanied ?) by the low-salinity gaseous, methane-dominated fluids at the transition from the retrograde skarn to hydrosilicate alteration stage (type 1B to type 2 fluid inclusions), and then again early during the phyllic alteration stage (type 3 to type 4 fluid inclusions). These data suggest cyclic fluid releases from crystallizing magma. Decreasing salinity of exsolved fluids corresponds to a trend of degassing that occurs in magmas crystallized at a greater depth (at greater pressure; >1.3 kbars), in contrast to that (from low- to high-salinity fluids) occurring in magmas crystallized at shallower depths (at lower pressure; <1.3 bars) (Shinohara and Hedenquist, 1997; Audetat et al., 2008). The full application of this model, however, is complicated by carbonic composition of the type 2 and 4 inclusions, as carbonic phase exsolves from magma first and at greater depth due to much lesser solubility (than that of H_2O and Cl) of carbonic species in granitic magmas (e.g., Lowenstern, 2001; Baker, 2002), and this incompatibility further enhances due to reduced nature of these carbonic fluids.

Consistently, it can be speculated that high-salinity aqueous fluids could be entirely or in part supplied from crystallizing granitoid magma, whereas reduced high-carbonic fluids – from a mafic magma source situated at a greater depth. Mixing of these two fluids may also have led to boiling. At the phyllic alteration stage, the incursion of highly-carbonic fluids from a mafic magma source may explain the enrichment of Au (together with Bi, As, Te, Sb, P, and F). The role of deeper mafic magma chambers adding metals and volatiles to granitoid-related mineral systems, or triggering magma-fluid separation through magma mixing, is recognized at many porphyry Cu-Au-Mo (Keith et al., 1998; Maughan et al., 2002; Muller and Groves, 2016), vein Au and polymetallic (Seifert, 2010), greisen Sn-W-Li (Seifert, 2010; Stemprok and Seifert, 2011), and skarn W-Mo-Cu (Soloviev, 2011, 2015) deposits, where mineralization overprints dikes of mafic rocks including lamprophyre intruded after emplacement of granitic phases. Rasmussen et al. (2011) suggested the same role of deeper mafic magma chambers producing post-mineralization shoshonitic lamprophyre dikes at the CanTung W skarn deposit, and this case has particular relevance to Lermontovskoe, where similar dikes post-date mineralization. Sulfur isotope data are consistent with a progressively greater

mantle input from hydrosilicate ($\delta^{34}S$ = -7.5 to -6.0 ‰) through early phyllic ($\delta^{34}S$ = -5.6 to -5.3 ‰) to late phyllic (to $\delta^{34}S$ = -5.5 to -4.4 ‰) alteration (Table 8) (Ohmoto and Goldhaber, 1997; Seal, 2006).

An abundant Au (+As, Bi, Te, Sb) mineralization at Lermontovskoe and other W-Au-base metal skarn and skarn/stockwork deposits of the Central Sikhote-Alin (Soloviev and Krivoschekov, 2011; Soloviev et al., 2017; Soloviev and Kryazhev, 2017) differs these deposits from some other reduced W skarn deposits such as CanTung and MacTung in Canada, which are "pure" W members. This can reflect signatures of the respective igneous suites in the Central Sikhote-Alin that are transitional between those of the "pure" reduced W and Au deposits, and suggests a continuum of W, W-Au, and Au (±W) deposits in the reduced W-Au deposit class.

On the other hand, the Au grades at Lermontovskoe are lower than those at some other W-Au-base metal skarn deposits of the Sikhote-Alin (Soloviev and Krivoschekov, 2011; Soloviev et al., 2017). This may in part reflect a deeper erosion level of the Lermontovskoe deposit that is supported by limited (~120-150 m) down-dip extent of mineralization that occurs in the near-contact zones of a relatively large granitoid intrusion. The intrusive rocks of the Lermontovskoe stock have just weakly-expressed porphyry (but mostly equigranular) texture, indicating that a deep (likely deep hypabissal) level of the pluton is now exposed. Fluid inclusion data revealed high (~1100-1400 bars) pressures corresponding to the lithostatic depth of >4-6 km from the paleosurface (Fournier, 1999) (Fig. 14). The deposit is characterized by coarse-grained muscovite-quartz phyllic alteration assemblages formed at high temperatures (>450^{o}C) that are typical for the root levels of porphyry and related deposits (Seedorf et al., 2008). Consistently, the Lermontovskoe deposit probably represents a root level of reduced W skarn deposits. This setting differs from that of the Vostok-2 W-Au-base metal skarn deposit (Soloviev and Krivoschekov, 2011; Soloviev et al., 2017), where subvertical zones of mineralized skarns (extending to hundreds of meters down-dip) are related to a small granodiorite-porphyry stock, containing intrusive breccias and likely representing a less eroded reduced intrusion-related W-Au system. The uppermost level of this system may be represented by the Skrytoe W skarn/stockwork deposit (Soloviev and Kryazhev, 2017), where W stockworks occur well above an uneroded intrusive, in zones of small granitoid and mafic dikes; large Au (±W) concentrations (e.g., the Malinovskoe Au deposit) are also present in the mineralized district. Thus, there can also be a continuum in structural settings of the deposits,

with a possible vertical geochemical model that implies W concentration at deeper (proximal) levels, and Au concentration at higher, most distal from causative intrusion, levels.

9. Conclusions

The Lermontovskoe deposit lies in a W-Sn-Au metallogenic belt formed in a collisional tectonic environment. It has low but consistent Au grades with elevated As, Bi, Te, and Sb suggesting a link to the reduced intrusion-related Au±W deposit class. The deposit is related to an ilmenite-series high-K peraluminous granodiorite-granite intrusion formed via mantle magma-induced melting of crustal sources.

The deposit incorporates reduced-type, pyroxene-dominated prograde and retrograde skarns overprinted by hydrosilicate (amphibole-chlorite-pyrrhotite-scheelite-quartz) and phyllic (muscovite/sericite-carbonate-albite-quartz-scheelite-sulfide, with abundant apatite) alteration assemblages. Early skarn mineralization is marked by high-temperature (>500^{o}C), high-pressure (1400-1500 bars) and high-salinity (53-60 wt.% NaCl-equiv.) magmatic-hydrothermal fluids and was followed by high-carbonic, methane-dominate, low-salinity fluid at the hydrosilicate alteration stage. Hydrosilicate alteration fluid boiled at 360-380^{o}C and 1300-1400 bars in zones of intense W mineralization. Phyllic alteration commenced with a high-temperature (>450^{o}C), high-pressure (1000-1100 bars) and high-salinity (42-47 wt.% NaCl-equiv.) magmatic-hydrothermal fluid, accompanied by high-carbonic, methane-dominated, low-salinity fluid that boiled at 390-420^{o}C and 1150-1200 bars in zones of most intense W mineralization. Following a significant pressure drop (to 370-400 bars), the late phyllic alteration is marked by lower-temperature (340-360^{o}C) high-carbonic, methane-dominated (but with higher CO_2 fraction), low-salinity fluid, and then a low-temperature (250-300^{o}C) H_2O-CO_2-CH_4-NaCl fluid. Both fluids boiled at the deposit level. During the overall fluid evolution, high-salinity aqueous fluids could have come from crystallizing granitoid magma, whereas the reduced high-carbonic fluids more likely came from a deeper mafic magma source. The latter could be a source of Au as well as Bi, As, Te, Sb, P, and F). Lower temperatures, high $a\mathrm{Ca}^{2+}$ and fluid boiling promoted scheelite deposition at all post-skarn hydrothermal stages.

The deposit has limited down-dip extent and this is interpreted to reflect the root zones of the reduced W-Au magmatic-hydrothermal system. The deep hypabyssal level of the intrusion, high-temperature, high-pressure and high-salinity fluids exsolved directly from crystallizing magma, abundance of coarse-grained

muscovite-quartz (+apatite, scheelite) aggregates in phyllic alteration, high aCa^{2+} (facilitating precipitation of scheelite), and limited Au mineralization further support this interpretation.

Acknowledgments

This paper represents part of the authors' work on research and assessment of W, Au and other deposits in Russia and Central Asia. Editorial reviews by Carl Brauhart and Franco Pirajno significantly improved the paper.

REFERENCES

Atkinson, A.B., 2002. A model for the PTX properties of H_2O-NaCl. Mc.Thesis, Virginia Tech. Inst. and State Univ., 126 p.

Audetat, A., Pettke, T., Heinrich, C.A., Bodnar, R.J., 2008. The composition of magmatic-hydrothermal fluids in barren and mineralized intrusions. Econ Geol 103, 877-908.

Baker, T., 2002. Emplacement depth and carbon dioxide-rich fluid inclusions in intrusion-related gold deposits. Econ. Geol. 97, 1111–1117.

Baker, T., Lang, J.R., 2003. Reconciling fluid inclusion types, fluid processes, and fluid sources in skarns: an example from the Bismark deposit, Mexico. Miner. Deposita 38, 474-495.

Baker, T., Pollard, P.J., Mustard, R., Mark, G., Graham, J.L., 2005. A comparison of granite-related tin, tungsten, and gold-bismuth deposits: implications for exploration. SEG Newsletter 61, 5-17.

Bakker, R.J., 2003. Package FLUIDS 1. Computer programs for analysis of fluid inclusions data and for modeling bulk fluid properties. Chem. Geol. 194, 3-23.

Becker, S.P., Fall, A., Bodnar, R.J., 2008. Synthetic fluid inclusions. XVII. PVTX properties of high-salinity H_2O-NaCl solutions (>30 wt.% NaCl): applications to fluid inclusions that homogenize by halite disappearance from porphyry copper and other hydrothermal ore deposits. Econ. Geol. 103, 539-544.

Belyansky, G.S., Rybalko, V.I., Syasko, A.A., Bazhanov, V.A., Uglova, N.I., Abramova, V.A., Oleinikov, A.B., Kovalenko, S.V., Kashtaev, B.I., Alenicheva, A.A., Gonokhova, N.G., 2011. Explanatory notes to the geological map of Russia, L-52/53, and K-52/53 map sheets, 1:1,000,000 scale, 3rd generation. VSEGEI, St-Petersburg. 699 p. (in Russian)

Bodnar, R.J., 1995. Fluid inclusion evidence for a magmatic source for metals in porphyry copper deposits. In: Thompson, J.F.H. (ed.): Magmas, Fluids, and Ore Deposits. Min. Assoc. Canada Short Course Series 23, 139-152.

Bodnar, R.J., Vityk, M.O., 1994. Interpretation of microthermometric data for H_2O-NaCl fluid inclusions. In: De Vivo, B., Frezzotti, M.L. (eds) Fluid inclusions in minerals, methods and applications. Blacksburg, Virginia Tech, p.117-130.

Bottrell, S.H., Yardley, B.D.W., Buckley, F., 1988. A modified crush-leach method for the analysis of fluid inclusion electrolytes. Bulletin de Minéralogie 111, 279-290.

Bowman, J.R., Covert, J.J., Clark, A.H., Mathieson, G.A., 1985. The Cantung E-Zone scheelite skarn orebody, Tungsten, Northwestern Territories: oxygen, hydrogen and carbon isotope studies. Econ. Geol. 80, 1872-1895.

Burruss, R.C., 1981. Analysis of phase equilibria in C-O-H-S fluid inclusions. In: Hollister, L.S., Crawford, M.L. (eds.) Fluid inclusions: Application to Petrology: Miner. Assoc. of Canada Short Course Handbook: Calgary 6, 39-74.

Burt, D.M., 1981. Acidity-salinity diagrams – application to greisen and porphyry deposits. Econ. Geol. 76, 832-843.

Burton, J.C., Taylor, L.A., Chou, I.-M., 1982. The fO_2-T and fS_2-T stability relations of hedenbergite and of hedenbergite-johannsenite solid solutions. Econ. Geol. 77:764-783.

Candela, P.A., Piccoli, P.M., 2005. Magmatic processes in the development of porphyry-type ore systems: Econ. Geol. 100^{th} Anniv. vol., 25-38.

Chappell, B. W., Bryant, C. J., Wyborn, D., 2012. Peraluminous I-type granites. Lithos 153, 142-153.

Cline, J.S., Bodnar, R.J., 1994, Direct evolution of brine from a crystallizing silicic melt at the Questa, New Mexico, molybdenum deposit. Econ. Geol. 89, 1780-1802.

Crawford, M.L., 1981. Phase equilibria in aqueous fluid inclusions. In Hollister LS, Crawford ML (eds) Fluid inclusions: Application to Petrology. Min Assoc Canada Short Course Handbook, Calgary 6, 75-100.

Dick, L.A., Hodgson, C.J., 1982. The MacTung W-Cu(Zn) contact metasomatic and related deposits of the North-eastern Canadian Cordillera. Econ. Geol. 77, 845-867.

Dolejs, D., Stemprok, M., 2001. Magmatic and hydrothermal evolution of Li-F granites: the Cinovec and Krasno intrusions, Krusne Hory batholiths, Chech republic. Bull. Chech Geol. Surv. 76, 77-99.

Drummond, S.E., Ohmoto, H., 1985. Chemical evolution and mineral deposition in boiling hydrothermal systems. Econ. Geol. 80, 126-147.

Einaudi, M.T., Meinert, L.D., Newberry, R.J., 1981. Skarn deposits. Econ. Geol. 75, 317-391.

Faure, G., 1986. Principles of Isotope Geology. 2nd edn. John Wiley & Sons Inc., New York. 608 p.

Fonteilles, M., Soler, P., Demange, M., Derre, C., Krier-Schellen, A.D., Verkaeren, J., Guy, B., Zahm, A., 1989. The scheelite skarn deposit of Salau (Ariege, French Pyrenees). Econ. Geol. 84, 1172-1209.

Fournier, R.O., 1999. Hydrothermal process related to movement of fluid from plastic into brittle rock in the magmatic-epithermal environment. Econ. Geol. 94, 1193-1212.

Gamble, R.P., 1978. An experimental study of sulfidation reactions involving andradite and hedenbergite. Econ. Geol. 77:784-797.

Gammons, C.H., Williams-Jones, A.E., 1997. Chemical mobility of gold in the porphyry-epithermal environment. Econ. Geol. 92, 45-59.

Gerstner, M.R., Bowman, J.R., Pasteris, J.D., 1989. Skarn formation at the McMillan Pass tungsten deposit (MacTung), Yukon and Northwest territories. 1. P-T-X-V characterization of the methane-bearing, skarn-forming fluids. Can Miner 27, 545-563.

Goldstein, R.H., Reynolds, T.J, 1994. Systematics of fluid inclusions in diagenetic minerals. Soc Sedim Geol Short Course 31

Gonevchuk, V.G., Gonevchuk, G.A., Korostelev, P.G., Semenyak, B.I., Seltmann, R., 2010. Tin deposits of the Sikhote-Alin and adjacent areas (Russian Far East) and their magmatic association. Austral. J. Earth Sciences 57, 777-802.

Gustafson, W.I., 1974. The stability of andradite, hedenbergite, and related minerals in the system Ca-Fe-Si-O-H. Jour. Petrol. 15, 455-496.

Guy, B., Faure, N., Le Loch, G., Varenne, J.-L., 1988. Etude microtermometrique des inclusions fluids des skarns a tungstene de Costabonne (Pyrenees, France): quelques resultants. C.R. Acad. Sci., Serie II, 307, 33-38.

Gvozdev, V.I., Ignatiev, A.I., Ukhaneva, N.G., Velivetskaya, T.A., 1999. Oxygen and carbon isotope composition of carbonates from scheelite skarn deposits of the Primorie region. Doklady Earth Sciences 367(5), 671-673.

Gvozdev, V.I., 2006. The Vostok-2 and Lermontovskoe deposits. In: The Large and Superlarge Ore Deposits. Moscow: IGEM RAN Publishing v.3, 627-667. (in Russian)

Gvozdev, V.I., 2007a. Ore-magmatic systems of scheelite-sulfide skarn deposits in the East of Russia. Sci. D. Thesis, Vladivostok: Far East Geol. Inst., 54 p. (in Russian)

Gvozdev, V.I., 2007b. Feldspathic metasomatic rocks from the Lermontovo deposit, Primorye, Russia. Geology Ore Deposits 49(3), 215-226.

Hart, C.J.R., 2007. Reduced intrusion-related gold systems. In Goodfellow, W.D. (ed.) Mineral deposits of Canada: A synthesis of major deposit types, district metallogeny, the evolution of geological provinces, and exploration methods. Geol Assoc Canada, Mineral Deposits Division, Spec Publ 5, 95-112.

Hart, C.J.R., Mair, J.L., Goldfarb, R.J., Groves, D.I., 2004. Source and redox controls on metallogenic variations in intrusion-related ore systems, Tombstone Tungsten Belt, Yukon Territory, Canada. Trans Roy. Soc. Edinburgh, Earth Sci. 95, 339-356.

Hedenquist, J.W., Arribas, A., Reynolds, T.J., 1998. Evolution of an intrusion-centered hydrothermal system: Far Southeast-Lepanto porphyry and epithermal Cu-Au deposits, Philippines. Econ. Geol. 93, 373-404.

Hunt, J.A., Kerrick, D.M., 1977. The stability of sphene: experimental determination and geologic implications. Geochim Cosmochim Acta 41, 279-288.

Ishihara, S., 1981. The granitoid series and mineralization. Econ. Geol. 75, 458-484.

Ishihara, S., 2004. The redox state of granitoids relative to tectonic setting and earth history: the magnetite-ilmenite series 30 years after. GSA Spec. Paper 389, 23-33.

Izosov, L.A., Vasilenko, N.G., Mel'nikov, N.G,, Petrishchevsky, A.M., 1988. Tungsten-bearing olistostrome of the Central Sikhote-Alin. Geotektonika 22, 76-87 (in Russian)

Jahn, B., Valui, G., Kruk, N., Gonevchuk, V., Usuki, M., Wu, J.T.J., 2015. Emplacement ages, geochemical and Sr–Nd–Hf isotopic characterization of Mesozoic to early Cenozoic granitoids of the Sikhote-Alin orogenic belt, Russian Far East: crustal growth and regional tectonic evolution. Jour. Asian Earth Sciences 111, 872-918.

Keith, J.D., Christiansen, E.H., Maughan, D.T., Waite, K.A., 1998. The role of mafic alkaline magmas in felsic porphyry Cu and Mo systems. In: Lentz, D.R. (Ed.), Mineralized intrusion-related skarn systems: Miner Assoc Canada Short Course 26, pp. 211-243.

Khanchuk, A.I., 2000. Paleogeodynamic analysis of the formation of ore deposits in the Russian Far East. In: Ore Deposits of Continental Margins, Vladivostok: Dal'nauka Publishing, p.5-34 (in Russian)

Khanchuk, A.I., Golozubov, V.V., Martinov, Yu.A., Simanenko, V.P., 1997. The Early Cretaceous and Paleogene transform continental margins (Californian type) of the Russian Far East. In: Tectonics of Asia, Moscow, GEOS, p.240-243 (in Russian)

Khetchikov, L.N., Pakhomova, V.A., Gvozdev, V.I., Zhuravlev, D.Z., 1998. Isotopic age of granitoids and ores of the Lermontovskoe scheelite-sulfide skarn deposit in the Central Sikhote-Alin (Russia). Geology Ore Deposits 40(1), 74-80.

Khetchikov, L.N., Pakhomova, V.A., Gvozdev, V.I., Zhuravlev, D.Z., 1999. Age of mineralization and some genetic features of the Vostok-2 scheelite-sulfide skarn deposit in the Central Sikhote-Alin. Ores and Metals 2, 30-36 (in Russian)

Kokorin, A.M., Kokorina, D.K., 1977. Temperature conditions of formation of the Lermontovskoe tungsten skarn-greisen deposit. In: Minerageny of Tin. The Far East Sci. Center of the USSR Sci. Acad., Vladivostok, pp.141-161. (in Russian)

Kontak, D.J., Kyser, K., 2011. A fluid inclusions and isotopic study of an intrusion-related gold deposit (IRGD) setting in the 380 Ma South Mountain Batholith, Nova Scotia, Canada: evidence for multiple fluid reservoirs. Min. Dep. 46, 337-363.

Korablinov, P.V., Degtyarev, V.M., Korablinova, N.I., 1984. Report on the detailed geological work completed in the western and central parts of the Lermontovskoe deposit area in 1981-1984. Unpubl. Prof. Report, USSR Geol. Surv. 355 p. (in Russian)

Korablinov, P.V., Nastich, N.A., 1975. The reserve calculation at the Lermontovskoe tungsten deposit. Unpubl. Prof. Report, USSR Geol. Surv. 675 p. (in Russian)

Korzhinskii, D.S., Pertzev, N.N., Zotov, I.A., 1984.Transmagmatic fluids and magmatogenic ore formation. A problem of mantle ore sources. In: Janelidze, T.V., Tvalchrelidze, A.G. (eds.) Proceedings of 6th Quadren. Symph. of International Association on the Genesis of Ore Deposits (IAGOD), Sept.6-12, 1982: Stuttgart, Nagele and Obermiller, v.1, p.131-138.

Kovalenko, V.I., Rub, M.G., Osipov, M.A., Gladkov, N.G., Efremova, S.V., Koval., P.V., Rub, A.K., Ryazantseva, M.D., Sherkhan, O., Yakimov, V.M., and Yarmolyuk, V.V., 1988. The Ore Potential of Igneous Associations, Moscow: Nauka Publishing, 231 p. (in Russian)

Kruk, N.N., Simanenko, V.P., Gvozdev, V.I., Golozubov, V.V., Kovach, V.P., Serov, P.A., Moskalenko, E.Yu., Kuibida, M.L., 2014. Geochemical characteristics and sources of the melts of the Early Cretaceous granitoids in the Samarga terrain (Sikhote-Alin). Russian Geology and Geophysics, no. 2, 276-302.

Kudrin, V.S., Kudrina, M.A., Silaev, A.E., Borodanov, V.M., 1979. Assessment of the new skarn scheelite occurrences adjacent to the Vostok-2 and Lermontovskoe deposits, and mineral composition of ores at deep levels of the Vostok-2 deposit. Unpubl. Prof. Report. Moscow, VIMS. 453 p. (in Russian)

Kwak, T.A.P., Tan, T.H., 1981. The importance of $CaCl_2$ in fluid composition trends – evidence from the King Island (Dolphin) skarn deposit. Econ. Geol. 76, 955-960.

Kwak, T.A.P., White, A.J.R., 1982. Contrasting W-Cu-Mo and W-Sn-F skarn types and related granitoids. Mining Geology 32, 339-351.

Lang, J.R., Baker, T., 2001. Intrusion-related gold systems: the present level of understanding. Miner Deposita 36, 477-489.

Lang, J.R., Stanley, C.R., Thompson, J.F.H., Dunne, K.P.E., 1995. Na-K-Ca magmatic-hydrothermal alteration in alkalic porphyry Cu-Au deposits, British Columbia. In: Thompson, J.F.H. (Ed) Magmas, fluids, and ore deposits. Min. Assoc. Canada Short Course Series 23, 339-366.

Lentz, D.R., Suzuki, K., 2000. A low F pegmatite-related skarn from the southwestern Grenville Province, Ontario, Canada: phase equilibria and petrogenetic implications. Econ. Geol. 95, 1319-1337.

Le Maitre, R.W., Bateman, P., Dudek, A., Keller, J., Lameyre, J., Le Bas, M.J., Sabine, P.A., Schmid, R., Sorensen, H., Streckeisen, A., Wooley, A.R., Zanettin, B., 1989. A classification of igneous rocks and glossary of terms. Blackwell, Oxford, 193 p.

Lowenstern, J.B., 2001. Carbon dioxide in magmas and implications for hydrothermal systems: Miner Deposita 36, 490-502.

Mair, J.L, Goldfarb, R.J., Johnson, C.A., Hart, C.J.R., Marsh, E.E., 2006. Geochemical constraints on the genesis of the Scheelite Dome intrusion-related gold deposit, Tombstone gold belt, Yukon, Canada. Econ. Geol. 101, 523-553.

Mair J.L., Farmer G.L., Groves D.I., Hart C.J.R., Goldfarb R.J., 2011. Petrogenesis of mid-Cretaceous post-collisional magmatism at Scheelite Dome, Yukon, Canada: evidence for a lithospheric mantle source for intrusion-related gold systems. Econ. Geol. 106, 451-480.

Maloof, T.L., Baker, T., Thompson, J.F.N., 2001. The Dublin Gulch intrusion-related gold deposit, Tombstone Plutonic Suite, Yukon Territory, Canada. Miner Dep 36, 583-593.

Maniar, P.D., Piccoli, P.M., 1989. Tectonic discrimination of granitoids. Geol. Soc. Amer Bull 101, 635-643.

Manning, D.A.C., Henderson, P., 1984. The behavior of tungsten in granitic melt-vapor systems. Contrib. Mineral. Petrol. 86, 286-293.

Masterman, G.J., Cooke, D.R., Berry, R.F., Walshe, J.L., Lee, A.W., Clark, A.H., 2005. Fluid chemistry, structural setting, and emplacement history of the Rosario Cu-Mo porphyry and Cu-Ag-Au epithermal veins, Collahuasi District, Northern Chile. Econ. Geol. 100, 835-862.

Mathieson, G.A., Clark, A.H., 1984. The CanTung E-Zone scheelite skarn orebody, Tungsten, Northwest Territories: a revised genetic model. Econ. Geol. 79, 883-901.

Maughan, D.T., Keith, J.D., Christiansen, E.H., Pulsipher, T., Hattori, K., Evans, N.J., 2002. Contributions from mafic alkaline magmas to the Bingham porphyry Cu-Au-Mo deposit, Utah, USA. Miner. Deposita 37, 14-37.

McCoy, D., Newberry, R.J., Layer, P., DiMarchi, J.J., Bakke, A., Masterman, J.S., and Minehane, D.L., 1997. Plutonic-related gold deposits of Interior Alaska. Econ Geol Monograph 9, 191-241.

Meinert, L.D., Dipple, G.M., Nicolesku, S., 2005, World skarn deposits. Econ. Geol. 100, 299-336.

Meinert, L.D., Hedenquist, J.W., Satoh, H., Matsuhisa, Y., 2003. Formation of anhydrous and hydrous skarns in Cu-Au ore deposits by magmatic fluids. Econ. Geol. 98, 147-156.

Middlemost, E.A.K., 1997. Magmas, Rocks and Planetary Development. Longman, Harlow, 299 p.

Muller, D., Groves, D.I., 2016. Potassic igneous rocks and associated gold-copper mineralization. Springer-Verlag, Berlin-Heidelberg-New York 4th edition, 311 p.

Mustard, R., Ulrich, T., Kamenetsky, V.S., Mernagh, T., 2006. Gold and metal enrichment in natural granitic melts during fractional crystallization. Geology 34, 85-88.

Newberry, R.J., 1983. The formation of subcalcic garnet in scheelite-bearing skarns. Can. Miner. 21, 529-544.

Newberry, R.J., 1998. W- and Sn-skarn deposits: a 1998 status report. In: Lentz, D.R. (ed) Mineralized intrusion-related skarn systems. Mineral Assoc Canada Short Course 26, 289-335.

Newberry, R.J., Swanson, S.E., 1986. Scheelite skarn granitoids: An evaluation of the roles of magmatic source and process. Ore Geol. Rev. 1, 57-81.

Ohmoto, H., Goldhaber, M.B., 1997. Sulfur and carbon isotopes. In: Barnes H.L. (ed.) Geochemistry of Hydrothermal Ore Deposits, 3rd edn. John Wiley and Sons, New York, p. 517-611.

Pearce, J., 1996. Sources and settings of granitic rocks. Episodes 19, 120-125.

Pirajno, F., 1992. Hydrothermal Mineral Deposits: Principles and Fundamental Concepts for the Exploration Geologist. Springer-Verlag, Berlin-Heidelberg-New York, 709 p.

Potter, R.W., 1977. Pressure corrections for fluid-inclusion homogenization temperatures based on volumetric properties of the system NaCl-H_2O. US Geol Surv Jour Research 5, 603-607.

Rafal'sky, R.P., Bryzgalin, O.V., Fedorov, P.L., 1984. Tungsten migration and scheelite deposition under hydrothermal conditions. Geochem. Internat 21, 1-13.

Rasmussen, K.L., Lentz, D.R., Falck, H., Pattison, D.R.M., 2011. Felsic magmatic phases and the role of late-stage aplitic dikes in the formation of the world-class Cantung tungsten skarn deposit, Northwest Territories, Canada. Ore Geol. Rev. 41, 75-111.

Robinson, B.W., Kusakabe, M., 1975. Quantitative preparation of sulfur dioxide, for $^{34}S/^{32}S$ analyses, from sulfides by combustion with cuprous oxide. Anal. Chem 47, 1179-1181.

Roedder, E., 1984. Fluid inclusions in minerals: Reviews in Mineralogy 12, 644 p.

Rub, M.G., Pavlov, V.A., Gladkov, N.G., Yashukhin, O.I., 1982. Tin- and Tungsten-bearing Granitoids in Some Regions of the USSR. Moscow: Nauka Publishing, 261 p. (in Russian)

Sakhno, V.G., Gvozdev, V.I., Alenicheva, A.A., Prasolov, E.M., Zarubina, N.V., 2012. Granitoid magmatism of the Lermontovskoe and Vostok-2 tungsten ore-magmatic systems: U-Pb dating (SHRIMP) and isotope characteristics of the ores. Doklady Earth Sciences 443(1), 84-91.

Sato, K., 1980. Tungsten skarn deposit of the Fujigatani mine, Southwest Japan. Econ. Geol. 75, 1066-1082.

Sato, K., Rodionov, S. M., Brublevsky, A. A., 2006. Lermontovskoe tungsten skarn deposit: the oldest mineralization in the Sikhote-Alin orogen, Far East Russia. Resource Geology 56(3), 257-266.

Schmidt, C., Bodnar, R.J., 2000. Synthetic fluid inclusions: XVI. PVTX properties in the system H_2O-NaCl-CO_2 at elevated temperatures, pressures, and salinities. Geochim. Cosmochim. Acta 64, 3853-3869.

Seal, R.R., 2006. Sulfur isotope geochemistry of sulfide minerals. Rev. Mineral. Geochem. 61, 633-677.

Seedorf, E., Barton, M.D., Stavast, W.J.A., Maher, D.J., 2008. Root zone of porphyry systems: extending the porphyry model to depth. Econ. Geol. 103, 939-956.

Seifert, T., 2010. Contributions to the metallogenetic importance of lamprophyres – examples from polymetallic Au-, Sn-W-Mo-Li-In-, As-Zn-Sn-Cu-In-Pb-Ag-/Ag-Sb-, and U-ore clusters. Mineralogia 37, 55-58.

Selby, D., Nesbitt, B.E., Muehlenbachs, K., 2000. Hydrothermal alteration and fluid chemistry of the Endako porphyry molybdenum deposit, British Columbia. Econ. Geol. 95, 183-202.

Seward, T.M., 1991. The hydrothermal geochemistry of gold: In: Foster, R.P. (ed.) Gold Metallogeny and Exploration: Glasgow, Blackies, p.165-209.

Shinohara, H., Hedenquist, J.W., 1997. Constraints of magma degassing beneath the Far Southeast porphyry Cu-Au deposit, Philippines. Jour. Petrology 38, 1741-1752.

Soloviev, S.G., 1997. Formation and location of tungsten skarn deposits in Phanerozoic orogenic belts. Unpubl. Sci. D. Dissertation, Moscow: VIMS, Moscow, 534 p. (in Russian)

Soloviev, S.G., 1999. Distribution types of REE in scheelites from skarns deposits. Doklady Earth Sciences 365(2), 252-255.

Soloviev, S.G., 2008. Metallogeny of Phanerozoic Tungsten Skarn Deposits. Scientific World Publishing, Moscow, 368 p. (in Russian)

Soloviev, S.G., 2011. Geology, mineralization, and fluid inclusion characteristics of the Kensu W-Mo skarn and Mo-W-Cu-Au alkalic porphyry deposit, Tien-Shan, Kyrgyzstan. Econ. Geol. 106, 193-222.

Soloviev, S.G., 2015. Geology, mineralization, and fluid inclusion characteristics of the Kumbel oxidized W-Cu-Mo skarn and Au-W stockwork deposit, Tien-Shan, Kyrgyzstan. Miner. Deposita 50, 187-220.

Soloviev, S.G., Krivoschekov, N.N., 2011. The Vostok-2 gold-base metal-tungsten skarn deposit, Central Sikhote-Alin, Russia. Geology Ore Dep. 6, 543-568.

Soloviev, S.G., Kryazhev, S.G., 2017, Geology, mineralization, and fluid inclusion characteristics of the Skrytoe reduced-type W skarn and stockwork deposit, Sikhote-Alin, Russia. Mineralium Deposita, 52 doi 10.1007/s00126-016-0705-1

Soloviev, S.G., Kryazhev, S.G., Dvurechenskaya, S.S., 2017, Geology, mineralization, stable isotope, and fluid inclusion characteristics of the Vostok-2 reduced W-Cu skarn and Au-W-Bi-As stockwork deposit, Sikhote-Alin, Russia. Ore Geology Reviews 86, 338-365.

Song, G., Qin, K., Li, G., Evans, N.J., Chen, L., 2014. Scheelite elemental and isotopic signatures: implications for the genesis of skarn-type W-Mo deposits in the Chizhou area, Anhui Province, Eastern China. Am. Miner. 99(2-3), 303-317.

Stemprok, M., 1987. Greisenization (a review). Geologische Rundschau 76, 169-175.

Stemprok, M., Seifert, T., 2011. An overview of the association between lamprophyric intrusions and rare-metal mineralization. Mineralogia 42, 121-162.

Stepanov, V.A., Gvozdev, V.I., 1987. Mineralogy and geochemistry of minor components in the ores of the skarn-scheelite deposits of the Far East. In: New Data on Mineralogy of the Far East. The Far East Division of the USSR Sci. Acad., Vladivostok, pp. 49-55.

Takagi, T., Naito, K., Collins, L.G., Iizumi, S., 2007. Plagioclase-quartz rocks of metasomatic origin at the expense of granitic rocks of the Komaki district, Southwestern Japan. Can. Mineralogist 45, 559-580.

Thiery, R., Kerkhof, A.M., Dubessy, J., 1994. vX properties of CH_4-CO_2 and CO_2-N_2 fluid inclusions: modeling for T <31ºC and P <400 bars. Eur. J. Mineral. 6, 753-771.

Thompson, J.F.H., Sillitoe, R.H., Baker, T., Lang, J.R., Mortensen, J.K., 1999. Intrusion-related gold deposits associated with tungsten-tin provinces. Miner. Dep. 34, 323-334.

Tooth, B., Brugger, J., Ciobanu, C., Liu, W., 2008. Modeling of gold scavenging by bismuth melts coexisting with hydrothermal fluids. Geology 36, 815-818.

Wood, S.A., Samson, I.M., 2000. The hydrothermal geochemistry of tungsten in granitoid environments: I. Relative solubilities of ferberite and scheelite as a function of T, P, pH, and mNaCl. Econ. Geol. 95, 143-182.

Wood, S.A., Vlassopoulos, D., 1989. Experimental determination of the hydrothermal solubility and speciation of tungsten at 500°C and 1 kbar. Geochim. Cosmochim. Acta53, 303-312.

Yang, X.-M., 2012. Sulfur solubility in felsic magmas: implications for genesis of intrusion-related gold mineralization. Geoscience Canada 39, 17-32.

Yuvan, J., 2006. Fluid inclusion and oxygen isotope studies of high-grade quartz-scheelite veins, CanTung mine, Northwest Territories, Canada: products of late-stage magmatic-hydrothermal event. M.Sc. Thesis, Univ Missouri-Columbia, 60 p.

FIGURE CAPTIONS

To the paper of S.G.Soloviev et al. "Geology, Mineralization, and Fluid Inclusion Characteristics of the Lermontovskoe Reduced-Type Tungsten (±Cu, Au, Bi) Skarn Deposit, Sikhote-Alin, Russia"

FIG. 1. Regional tectonic setting of the Lermontovskoe and other W and Au deposits of the Central Sikhote-Alin (Central Sikhote-Alin gold-tungsten-tin metallogenic belt). The geology is after Khanchuk et al. (1997); Khanchuk (2000); the deposit locations are after Belyansky et al. (2011), Stepanov et al. (2013).

FIG. 2. Geological setting of the Lermontovskoe mineralized district (modified after Korablinov et al., 1984; Gvozdev, 2006; Belyansky et al., 2011). Numbers in circles (Early Cretaceous plutons): 1 – Shivkinsky pluton, 2 – Lermontovskoe stock, 3 – Olympyisky pluton, 4 – Gorbunsky pluton.

FIG. 3. Geological map of the Lermontovskoe deposit area (modified after Korablinov and Nastich, 1975; Kudrin et al., 1979; Korablinov et al., 1984; Gvozdev, 2006).

FIG. 4. Classification diagrams illustrating the chemistry of the Early Cretaceous igneous rocks from the Lermontovskoe deposit. (A) SiO_2 vs. (K_2O+Na_2O) diagram (after Middlemost, 1997). (B) SiO_2 vs. K_2O diagram (after La Maitre et al., 1989). (C) Al/(Na+K) vs. Al/(Ca+Na+K) diagram defining the alkaline, meta-aluminous and peraluminous igneous rocks (after Maniar and Piccoli, 1989). (D) Rb vs. (Y+Nb) diagram showing compositional fields of granitic rocks formed in syncollisional (syn-COLG), post-collisional (post-COLG), volcanic arc (VAG), within-plate (WPG), and oceanic ridge (ORG) tectonic environments (after Pearce, 1996). Sample numbers (1-20) are from Table 2.

FIG. 5. Geological map of the Central mineralized zone of the Lermontovskoe deposit (modified after Korablinov and Nastich, 1975; Korablinov et al., 1984).

FIG. 6. Cross-sections of the Central mineralized zone of the Lermontovskoe deposit (modified after Korablinov and Nastich, 1975; Korablinov et al., 1984). For the legend see Fig. 5.

FIG. 7. Paragenesis of alteration mineral assemblages showing sequence of mineralization at the Lermontovskoe deposit in alternation with the intrusion phases.

FIG. 8. Photographs showing some typical features of rocks and hydrothermal alteration assemblages at the Lermontovskoe deposit. A. Banded prograde pyroxene-plagioclase skarn replacing alternating biotite hornfels-marble-quartzite sequence. B. Massive zoned prograde pyroxene-garnet skarn replacing massive marble (M); garnet (Grt) forms a rim most proximal to the marble, pyroxene (Px) is more distal. C. Marble (M) relict in retrograde pyroxene-quartz (with minor amphibole and pyrrhotite) skarn indicating the protolith. D. Hydrosilicate alteration assemblage with amphibole (Amp) and pyrrhotite (Po) replacing pyroxene skarn (Px). E. Massive pyrrhotite (with minor chalcopyrite) in zone of hydrosilicate alteration. F. Coarse-grained quartz-muscovite-carbonate-apatite-scheelite phyllic alteration zone overprinting granodiorite. G. Coarse scheelite (Sch) in quartz-muscovite-carbonate-apatite phyllic alteration zone overprinting granodiorite. H. Massive coarse-crystalline arsenopyrite (Apy) in zone of phyllic alteration. I. Scheelite-apatite-arsenopyrite-quartz veinlets cutting biotite hornfels. J. An external phlogopite-rich zone of quartz-muscovite-carbonate-apatite phyllic alteration (with long-prismatic apatite crystals; Ap) overprinting pyrrhotite-rich hydrosilicate alteration. K. An internal quartz-scheelite zone of phyllic alteration. L. Large apatite crystals (light-green; Ap) growing through scheelite (light-yellow; Sch). M. Quartz-sericite-sulfide (pyrrhotite, scheelite) assemblage of phyllic alteration. Abbreviations: Grt – garnet, Px – pyroxene, Amp – amphibole, Qz – quartz, Phl – phlogopite, Apy – arsenopyrite, Po – pyrrhotite, Sch – scheelite, Ap – apatite.

FIG. 9. Photomicrographs of thin and polished sections showing relationships of minerals at the Lermontovskoe deposit. A. Pyrrhotite intensely replaces fine-grained pyroxene of prograde skarn but the large retrograde skarn pyroxene crystal is euhedral and is just partially replaced by pyrrhotite indicating nearly-contemporaneous growth of pyroxene and pyrrhotite in retrograde skarn (thin section, nicols crossed). B.

Anhedral scheelite and pyroxene of retrograde skarn are corroded by amphibole-pyrrhotite-calcite-quartz assemblage of hydrosilicate alteration (thin section). C. Euhedral scheelite crystal in amphibole-pyrrhotite assemblage of hydrosilicate alteration (thin section, nicols crossed). D. Ca-plagioclase, phlogopite, pyrrhotite and scheelite in the outer zone of hydrosilicate alteration (thin section). E. Phlogopite, sulfides and fine-grained apatite in the outer zone of phyllic alteration (thin section). F. Carbonate, muscovite and apatite in the intermediate zone of phyllic alteration (thin section, nicols crossed). G. Coarse scheelite, muscovite and quartz in the central (core) zone of phyllic alteration (thin section, nicols crossed). H. Apatite intergrowing scheelite and quartz (phyllic alteration) (thin section, nicols crossed). I. Pyrrhotite is replaced by arsenopyrite, and then both are replaced by sphalerite and chalcopyrite in phyllic alteration assemblage (polished section). J. Scheelite grows through arsenopyrite with pyrrhotite relicts in phyllic alteration assemblage (polished section). K. Scheelite grows through chalcopyrite but contains thin chalcopyrite veinlets in phyllic alteration assemblage (polished section). L. Scheelite, chalcopyrite, pyrrhotite and sphalerite, and also apatite in phyllic alteration assemblage (polished section). Abbreviations: Sch – scheelite, Ap – apatite, Po – pyrrhotite, Ccp – chalcopyrite, Sp – sphalerite, Qz – quartz, Phl – phlogopite, Pl – plagioclase, Px – pyroxene, Cb - carbonate.

FIG. 10. Photomicrographs of polished sections showing relationships of Bi and Au minerals in the phyllic assemblage at the Lermontovskoe deposit. A. Chalcopyrite and native bismuth in the interstitions of arsenopyrite crystals. B. Pyrite, native bismuth, pyrrhotite and galena inclusions in arsenopyrite. C. Galena and native bismuth in the interstitions of arsenopyrite crystals. D-E. Galena, native bismuth and native gold replacing arsenopyrite (E – larger view). F-G. Large scheelite crystal in fine-grained pyrrhotite-chalcopyrite aggregate contains inclusions and veinlets of chalcopyrite, pyrrhotite and native bismuth with bismuth tellurides (G – larger view). H-J. Bismuth minerals and native gold associated with sphalerite and chalcopyrite (I-K – larger views: I – native bismuth and hedleyite, J – native gold, K – native bismuth, bismuthinite and tellurobismuthite). L. Sphalerite with veinlets of chalcopyrite, native bismuth and Bi tellurides. M. Chalcopyrite-pyrrhotite aggregate is replaced by native bismuth and hedleyite. N-O. Sphalerite-pyrrhotite-chalcopyrite veinlets with bismuth minerals (O – larger view; native bismuth and hedleyite; nicols crossed). P. Sphalerite, native bismuth and pyrrhotite. Abbreviations: Qz – quartz, Sch – scheelite, Py – pyrite, Po –

pyrrhotite, Apy – arsenopyrite, Ccp – chalcopyrite, Sp – sphalerite, Gn – galena, Au – native gold, Bi – native bismuth, TeBi – tellurobismuthite, Hd - hedleyite.

FIG. 11. Types of fluid inclusions in minerals from various hydrothermal alteration assemblages at the Lermontovskoe deposit. A-B. Individual multisolid type 1A inclusion in prograde skarn garnet (B – larger view). C-D. Multiphase (with halite) type 1B inclusions in retrograde skarn pyroxene (D – larger view). E-F. Carbonic type 2A and aqueous-carbonic type 2B inclusions in quartz of hydrosilicate alteration assemblage (long prismatic crystals – amphibole). G-H. Aqueous-carbonic type 2B inclusions in scheelite of hydrosilicate alteration assemblage (H – larger view). I. Homogenization-heterogenization of the type 2A carbonic fluid inclusion under cooling-warming at -150 to -85^{o}C. J-M. Multisolid (with large halite crystal) type 3 inclusions in quartz of the early assemblage of phyllic alteration (K, M – larger views). N-O. Carbonic type 4A and aqueous-carbonic type 4B inclusions in scheelite of the early assemblage of phyllic alteration (O – larger views). P. Homogenization-heterogenization of the type 4A carbonic fluid inclusion under cooling to -90^{o}C. Q. Carbonic type 5A and aqueous-carbonic type 5B inclusions in quartz of the late assemblage of phyllic alteration. R. Homogenization-heterogenization of the type 5A carbonic fluid inclusion under cooling-warming at -80 to -65^{o}C. S. Gaseous-liquid type 6A and multiphase (with halite) type 6B inclusions in quartz of the late assemblage of phyllic alteration. T-U. Gaseous-liquid type 6A and multiphase (with halite) type 6B inclusions in apatite of the late assemblage of phyllic alteration (U – larger view).

FIG. 12. A. Frequency histograms of final homogenization temperatures for various fluid inclusion types in minerals from the hydrosilicate and phyllic alteration assemblages of the Lermontovskoe deposit. (B-C) Pressure (shaded areas) estimates for the formation conditions of the retrograde skarn (type 1A fluid inclusions) (B) and phyllic alteration assemblages (type 3 fluid inclusions) (C). Vapor pressure curves and halite liquidus lines (labelled in wt.% NaCl) as well as the three-phase (L+V+H) curve for the NaCl-H_2O system are from Becker et al. (2008), Atkinson (2002). These vapor pressure curves and halite liquidus lines correspond to most common salinities of the halite-bearing fluid inclusions in the retrograde skarn (type 3 fluid inclusions) and phyllic alteration assemblage (type 4A fluid inclusions) determined in this study (30-50 wt.% NaCl-equiv.).

FIG. 13. Compositions of the igneous rock from the Lermontovskoe deposit shown on the schematic plot of degree of fractionation (Rb/Sr ratio) versus the oxidation state (Fe_2O_3/FeO) for intrusive rocks associated with Cu-Au, W-Mo, W, Au-(Bi) and Sn mineralization (Baker et al., 2005). Sample numbers (1-20) are from Table 2.

FIG. 14. Estimated pressure and temperature conditions and evolutional paths for different fluid inclusion types (1-6) in hydrothermal assemblages at the Lermontovskoe deposit, with composition of different fluid inclusion types as a function of depth and temperature (after Hedenquist et al., 1998; Fournier, 1999; Meinert et al., 2003; Baker and Lang, 2003). Vapor-pressure curves for H_2O-NaCl solutions at 0-70 wt.% NaCl-equiv. and the three-phase (L+V+H) curve are shown after Atkinson (2002), Becker et al. (2008). Curved lines labelled 1 and 2 represent the dry solidus of a quartz monzonite and solubility of a granite bearing 2 wt.% fluorine, respectively (Selby et al., 2000). The two-phase (L/L+V) curve for H_2O-NaCl-CO_2 fluid containing 6 wt.% NaCl and 4.08 mol.% CO_2 (Schmidt and Bodnar, 2000) is shown. PT-fields for the major fluid inclusion types and possible evolutional paths for fluids (shaded arrows) are shown.

Table 1. Major Petrographic Features of Igneous Rocks from the Lermontovskoe Intrusive Stock

Phase	Rocks	Petrography
1	Monzonite to tonalite	Medium- to fine-grained equigranular grey rock composed of brownish-green amphibole (2-7 vol.%), dark-brown to reddish-brown biotite (10-15 vol.%), plagioclase (10-55 vol.%), K-feldspar (orthoclase) (10-25 vol.%), and quartz (10-15 vol.%). Accessory minerals – apatite, zircon, rutile, titanite, and ilmenite.
2	Granodiorite	Medium- to fine-grained equigranular to weakly-porphyry grey rock composed of brownish-green amphibole (0-3 vol.%), dark-brown to reddish-brown biotite (5-10 vol.%), plagioclase (35-45 vol.%), K-feldspar (orthoclase) (20-25 vol.%), and quartz (20-25 vol.%). Plagioclase is represented by two generations: larger (up to 2 mm) crystals zoned from labradorite (with 55-60 mol.% anorthite) in the core to andesine-oligoclase (with 40-20 mol.% anorthite) in the rims, and small tabular crystals in the groundmass composed of andesine-oligoclase (with 30-25 mol.% anorthite). K-feldspar locally contains small perthite (oligoclase and albite) intergrowths. Biotite is also represented by two generations: larger (up to 1.5 mm) crystals corroded by K-feldspar and quartz, and small (<0.5 mm) flakes interstitial to other minerals. Biotite contains numerous small euhedral crystals of accessory apatite, zircon, monazite, ilmenite, and rutile. Acicular apatite crystals are present in plagioclase, whereas prismatic apatite crystals are associated with biotite. Other accessory minerals include scheelite, titanite, rare cordierite and pink garnet, and trace magnetite.
3	Granite	Fine-grained equigranular light-grey rock composed of dark-brown to reddish-brown biotite (2-5 vol.%), plagioclase (25-35 vol.%), K-feldspar (orthoclase) (25-30 vol.%), and quartz (30-35 vol.%). Plagioclase is represented by two generations: larger (up to 2 mm) crystals zoned from andesine (with 35-45 mol.% anorthite) in the core to andesine-oligoclase (with 30-20 mol.% anorthite) in the rims, and small tabular crystals in the groundmass composed of oligoclase (with 27-22 mol.% anorthite). Accessory minerals include apatite, zircon, rutile, ilmenite, titanite and scheelite.
4	Leucogranite-aplite (dikes)	Fine-grained leucocratic light-grey to white rock composed of K-feldspar (30-40 vol.%), oligoclase-andesine with 25-35 mol.% anorthite (25-35 vol.%), quartz (30-35 vol.%), and biotite (1-3 vol.%). Accessory minerals include apatite, ilmenite, zircon, and scheelite.
5	Monzogabbro-porphyry (“lamprophyre”) (dikes)	Fine-grained dark-grey to dark greenish-grey rock composed of plagioclase (50-60 vol.%), K-feldspar (orthoclase (0-5 vol.%), greenish-brown amphibole (15-25 vol.%), and dark brown to reddish-brown biotite (10-15 vol.%). Plagioclase phenocrysts are long-prismatic, polysynthetic-twinned, and zoned from labradorite (55-60% anorthite) core to andesine rim; plagioclase in the groundmass is represented by andesine (45-48% anorthite). Accessory minerals – apatite, zircon, titanite, and ilmenite.

Table 2. Chemical Compositions of Igneous Rocks from the Lermontovskoe Deposit (wt.%, ppm)

	Monzonite to tonalite		Granodiorite										Granite			Leucogranite			Monzogabbro-porphyry ("lamprophyre")	
	1	2(2)	3(3)	4	5	6(11)	7	8(18)	9	10	11	12	13(3)	14(2)	15	16	17	18	19	20
wt percent																				
SiO_2	61.20	61.40	66.43	67.16	67.48	68.11	68.30	68.57	68.96	69.20	69.33	69.40	70.54	71.24	72.00	74.70	74.90	75.17	48.56	50.67
TiO_2	0.87	0.92	0.60	0.60	0.57	0.51	0.53	0.51	0.48	0.44	0.50	0.45	0.34	0.26	0.28	0.12	0.12	0.23	1.12	0.74
Al_2O_3	16.10	17.63	15.89	16.02	15.88	15.25	15.83	14.96	15.23	15.20	15.08	15.29	15.16	15.34	13.90	13.60	13.40	13.24	16.12	14.62
Fe_2O_3	1.75	1.02	0.49	0.81	1.01	0.93	1.01	0.88	1.05	0.90	0.80	1.03	0.74	0.41	0.53	0.46	0.48	0.41	2.99	2.78
FeO	4.32	4.82	3.79	3.90	3.12	3.06	2.91	2.94	2.83	2.50	2.70	2.31	2.08	2.32	2.05	0.53	0.63	0.76	6.41	6.15
MnO	0.11	0.08	0.04	0.07	0.06	0.07	0.05	0.07	0.04	0.04	0.05	0.04	0.05	0.05	0.05	0.05	0.05	0.06	0.16	0.14
MgO	2.50	2.81	1.79	1.76	1.70	1.33	1.64	1.43	1.38	1.38	1.50	1.13	1.19	1.14	1.12	0.30	0.32	0.32	7.17	8.20
CaO	4.83	2.83	2.67	0.81	0.92	1.82	0.88	1.44	0.99	1.56	1.12	0.89	0.83	0.98	1.40	0.54	0.48	0.66	7.19	8.28
Na_2O	3.15	2.83	2.93	2.86	2.88	3.04	2.92	3.07	2.80	3.29	3.05	3.00	3.11	3.16	3.80	3.48	3.52	3.86	3.52	2.09
K_2O	3.95	2.83	3.60	3.37	3.50	3.47	3.55	3.63	3.53	3.08	3.41	3.75	4.07	3.92	4.17	4.79	5.12	5.23	1.82	1.77
P_2O_5	0.25	0.23	0.26	0.15	0.16	0.21	0.15	0.17	0.21	0.15	0.19	0.15	0.13	0.14	0.13	0.28	0.32	0.24	0.30	0.23
CO_2				<0.20	<0.20		<0.20		0.44	<0.20	<0.20	0.26		0.47		<0.20	<0.20	<0.20	0.75	<0.20
S tot.				0.43	0.32		0.47		0.10	0.47	0.60	0.15				<0.10	<0.10	<0.10	<0.10	<0.10
F		0.24		0.07	0.10		0.14	0.29	0.13	0.12	0.13	0.13		0.20		0.020	0.018	0.013	0.11	0.085
H_2O^-				0.16	0.20		0.25	0.00	0.25	0.22	0.30	0.41		0.07	0.12	0.15	0.22	0.17	0.43	0.78
H_2O^+				0.89	0.94		1.08	1.13	1.29	0.93	0.69	0.65		0.92		0.32	0.36	0.28	3.33	3.61
L.O.I.	0.35	2.23	1.34			2.07							2.12		0.58					
Total	99.40	99.87	99.30	99.26	99.04	100.17	99.91	99.09	99.71	99.68	99.65	99.04	100.23	100.62	100.31	99.64	100.14	100.94	100.08	100.45
ppm																				
Ba	660			612	598		553		545	563	589	652				312	243	244	491	589
Sr	422			202	180		175		142	168	174	184				140	124	162	532	410
Co				10	8.0		5.8		7.9	7.4	7.1	6.5				2.4	1.8	1.5	35	35
Ni				36	32		28		47	45	30	52				12	12	14	53	69
V	110			54	48		40		47	50	46	37				11	11	13	290	200
Li				63	52		32	34	26	30	28	29		30		15	18	12	43	29
Rb	139			137	140		145	149	136	109	127	127		185		176	154	123	69	55
Be				2.2	2.2		2.6		3.3	5.1	3.5	2.6				3.8	4.0	4.2	2.8	2.1
Zr	233			182	180		175		160	155	178	141				122	132	128	107	88
Nb	16.1			14	15		15		13	9.8	14	11				15	16	16	7.0	6.3
Y	22.5			12	12		15		15	15	15	15				12	15	12	30	15
B				20	22		15		20	20	15	15				12	15	15	10	10
Sn				14	16		17		19	13	24	23				12	18	7	<5	<5
Mo				2.8	2.8		1.2		5.2	3.8	1.9	4.6				2.0	2.0	2.5	3.2	3.2
Cu				50	40		40		30	40	40	40				20	20	20	60	40
Zn				40	60		60		60	40	60	60				20	30	20	15	10
Pb	18.4			20	30		15		20	20	12	15				20	30	20	10	8
W				1.6	1.8		8.0	4.2	1.7	12.3	7.1	1.6		3.4		6.2	4.4	3.5	1.1	0.8
Kd	12.7	12.8	17.5	19.3	20.3	20.0	20.9	20.7	21.3	20.7	21.2	22.6	23.5	22.5	23.3	27.0	27.1	28.5	-2.8	-4.0

Sample 1 – data from Sakhno et al. (2012), samples 2, 3, 6, 13, 15 – from Gvozdev (2007), samples 8, 14 – from Rub et al. (1982) (in brackets – number of samples for calculating averages by authors of the publications). For the other samples (4-5, 7, 9-12, 16-20) – analyses were performed in the Russian Analytical Centre (VIMS) Laboratories, Moscow. Most of the major oxides (SiO_2, TiO_2, Al_2O_3, $Fe_2O_{3\ total}$, MnO, MgO, CaO, K_2O, and P_2O_5) as well as Sr, Nb, and Zr were determined by X-ray fluorescence method using a multi-channel X-ray spectrometer. Supplementary determinations by wet chemical methods included FeO (volumetric method), Na_2O (flame photometry), F (ion chromatography), CO_2 (acidic titration), S_{total} (iodic titration), H_2O^+ (gravimetry). In addition, Li and Rb were also determined by flame photometric method. The ICP-ES method was used for determination of Ni, Co, V, Be, Sn, Mo, Y, B, Cu, Zn, and Pb. Also, X-ray radiometric method was used for determination of Ba, and neutron activation method – for determination of W. Detection limits: SiO_2 – 0.50 wt.%, TiO_2 – 0.02 wt.%, Fe_2O_3 and FeO – 0.25 wt.%, MgO, CaO, Na_2O, K_2O and CO_2 – 0.20 wt.%, P_2O_5 – 0.04 wt.%, H_2O and $S_{tot.}$ – 0.10 wt.%, MnO and F - 0.02 wt.%, Ba, Sr, and Zr – 20 ppm, Co, V, Nb, Sn, Y and Rb – 5 ppm, Li, B, Cu, Zn, Pb, and Ni – 1 ppm, Be, Mo, and W – 0.1 ppm. Kd – differentiation coefficient (index) (Larson index = $1/3SiO_2 + K_2O – (FeO+CaO+MgO)$).

Table 3. Rare and Rare Earth Element Contents in Selected Samples of the Igneous Rocks from the Lermontovskoe Stock (ppm)

	1	5	7
Cr		33.1	38.9
Sc		7.7	8.7
Ta		0.87	1.14
Hf		5.47	5.12
Cs		7.1	6.2
Th	12.5	10.74	11.95
U	2.32	2.79	4.41
La	31.1	29.1	34.7
Ce	63.6	63.8	76.5
Nd	26.2	26.9	33.4
Sm	5.28	5.25	6.34
Eu	1.14	0.93	1.03
Tb	0.70	0.69	0.87
Yb	2.17	1.71	2.18
Lu	0.31	0.26	0.30
$(La/Yb)_N$	9.7	11.6	10.8

Sample 1 – data from Sakhno et al. (2012). For samples 5-7 - assaying was performed in the Russian Institute of Experimental Mineralogy (IEM RAN), Chernogolovka, by instrumental neutron activation method. 100-mg samples were irradiated together with a standard by a thermal neutron flux of 1.2×10^{13} n/cm^2 × s during 20 hr. REE fractions were separated by radiochemical method. Gamma-spectrometry determination of REE was done with a coaxial Ge(Li)-detector. The accuracy of the analyses for individual elements is: ±3%-5% for La, Sm, Eu, Yb, and Lu, ±5%-7% for Ce, Tb, and ±10% for Nd. Sample numbers are from Table 2.

Table 4. Representative Microprobe Analyses of Pyroxene, Garnet and Amphibole from the Lermontovskoe Deposit, wt.%, mol.%

Mineral	Pyroxene				Garnet				Amphibole			
Assemblage	Prograde skarn		Retrograde skarn		Prograde skarn		Retrograde skarn		Retrograde skarn		Hydrosilicate alteration	
	1	2	3	4	5	6	7	8	9	10	11	12
SiO_2, wt.%	51.32	51.53	50.88	51.67	37.03	36.90	37.34	37.50	51.42	52.26	51.26	51.87
TiO_2, wt.%	0.43	0.51	0.46	0.34	0.23	0.21	0.21	0.14	0.51	0.60	0.62	0.67
Al_2O_3, wt.%	0.87	0.67	0.33	0.21	14.98	12.71	17.35	20.12	3.21	3.01	4.32	4.29
FeO, wt.%	19.82	21.02	22.93	23.87	12.73	15.04	12.68	13.16	21.23	20.84	16.43	14.00
MnO, wt.%	0.71	0.61	1.33	1.46	0.67	0.50	3.44	3.51	0.72	0.81	1.22	1.43
MgO, wt.%	3.89	4.81	1.21	0.56	0.28	0.24	0.32	0.22	8.41	7.32	11.43	12.08
CaO, wt.%	22.44	21.43	22.42	22.61	32.74	32.16	27.12	25.01	11.82	12.44	12.15	12.32
Na_2O, wt.%									0.22	0.32	0.43	0.56
K_2O, wt.%									0.35	0.30	0.33	0.32
H_2O, wt.%									2.00	2.00	2.04	2.06
Total, wt.%	99.48	100.58	99.56	100.72	98.68	97.76	98.46	99.66	99.89	99.90	100.23	99.60
	Di 27	Di 30	Di 6	Di 4	Alm 3	Alm 5	Alm 13	Alm 20				
	Hd 70	Hd 68	Hd 86	Hd 90	Adr 33	Adr 39	Adr 17	Adr 9				
	Jo 3	Jo 2	Jo 8	Jo 6	Grs 61	Grs 54	Grs 61	Grs 62				
					Prp 1	Prp 1	Prp 1	Prp 1				
					Sps 1	Sps 1	Sps 8	Sps 8				

Di=diopside, Hd=hedenbergite, Jo=johannsenite, Alm=almandine, Adr=andradite, Grs=grossular, Prp=pyrope, Sps=spessartine

1-2 – pyroxene from prograde skarn, 3-4 – pyroxene from retrograde skarn, 5-6 – garnet from prograde skarn, 7-8 – garnet from retrograde skarn, 9-10 – ferroactinolite from retrograde skarn replacing prograde pyroxene skarn, 11-12 – actinolite from hydrosilicate alteration assemblage replacing pyroxene skarn. The analyses were performed by Cameca SX50 microprobe in the Moscow State University, Russia, under operating conditions of 15 kV accelerating voltage, 30 nA beam current, with a beam diameter ~3 μm. The accuracy of element measurements was ±2% rel. for concentrations >10 wt.%, ±5% rel. for concentrations of 5-10 wt.%, ±10% rel. for concentrations of 1-5 wt.%, and ±15% rel. for concentrations of 0.1-1.0 wt.%.

Table 5. Mo and REE Contents in Scheelite from the Lermontovskoe Deposit (ppm)

samples	Mo	La	Ce	Nd	Sm	Eu	Tb	Yb	Lu	$(La/Yb)_N$
1	75	77.4	48.0	27.3	5.05	28.3	1.90	7.53	1.48	7.0
2	58	68.6	47.3	24.1	5.42	16.73	1.29	4.02	1.00	11.6

The samples of scheelite with blue luminescence are from the late (quartz-sericite-carbonate-sulfide-Bi-Au, with chalcopyrite and pyrrhotite) mineral assemblage of phyllic alteration. The instrumental neutron activation analysis method used is the same as in Table 3.

Table 6. Types of Fluid Inclusions (FI) in Minerals from Various Hydrothermal Assemblages of the Lermontovskoe Deposit

Mineral (number of FI measured)	FI type	FI size	FI content	T_m eu., °C	T_m CO_2, °C	T_m ice, °C	T_h carb, °C	T_m clathrate, °C	Homogenization, T_h, °C	Estimated salinity, wt.% NaCl-equiv.	Estimated CO_2/CH_4 ratio***	Estimated pressure, bars
Prograde pyroxene-garnet skarn												
Garnet (6)	1A	5-20 μm	Multisolid, no halite, 15-20 vol.% gas						Gas to liquid at 350-390			
Retrograde quartz-pyroxene skarn												
Pyroxene (8)	1B	5-20 μm	Multisolid, with halite, 30-60 vol.% gas						Gas to liquid at 310-350, halite at 450-500	53-60**		1400-1500*****
Quartz-amphibole-chlorite-pyrrhotite-scheelite hydrosilicate (propylitic) alteration assemblage												
Quartz, scheelite (40)	2A	5-25 μm	>95 vol.% gas				-88.0 - -90.0	+14.0 - +16.5			<0.01	1300-1400****
Quartz, scheelite (20)	2B	5-25 μm	30-40 vol.% gas						360-380 to liquid			
Early (quartz-muscovite-carbonate-apatite-scheelite-arsenopyrite) phyllic alteration assemblage												
Quartz, scheelite, carbonate (10)	3	5-25 μm	Multisolid, with halite, 10-20 vol.% gas						Gas to liquid at 250-290, halite at 350-400	42-47**		1000-1100*****
Quartz, scheelite (20)	4A	5-30 μm	65-85 vol.% gas				-83.0 - -85.0	+10.5 - +11.5	390-420 to gas		<0.01	1150-1200****
Quartz, scheelite (30)	4B	5-30 μm	15-25 vol.% gas	-25.0		-6.0 - -6.5		-7.2 - -5.0	390-420 to liquid	9.0-10.0*		
Late (quartz-sericite-carbonate-sulfide-Bi-Au) phyllic alteration assemblage												
Quartz (12)	5A	5-20 μm	70-80 vol.% gas		-67.0 - -64.5			+11.7 - +12.0	340-360 to gas		10:90	370-400****
Quartz (44)	5B	5-20 μm	15-25 vol.% gas	-26.0 - -24.2		-8.2 - -6.2			340-360 to liquid	9.5-12.0*		
Quartz (5)	6A	5-25 μm	>95 vol.% gas		-63.5		-12.0 - -18.0				50:50	300-350****
Quartz (30)	6B	5-25 μm	Multisolid, with halite, 20-25 vol.% gas				-		Halite at 200-230, gas to liquid at 250-300	32-34**		

T_m eu. – eutectic temperature (first ice melting temperature), °C; T_m carb – final CO_2 melting temperature, °C; T_m ice - final ice melting temperature, °C; T_m clathrate - final clathrate melting temperature, °C; T_h carb – carbonic phase homogenization temperature, °C.

* Salinity estimated by final ice melting temperature (Bodnar and Vityk, 1994).

**Salinity estimated by halite melting temperature (Bodnar and Vityk, 1994).

***The ratio estimated by final CO_2 melting temperature and carbonic phase homogenization temperature (Thiery et al., 1994).

****The trapping pressure estimated by using the T_h of type B and the density of type A fluid inclusions trapped contemporaneously. The density was determined by final CO_2 melting temperature and carbonic phase homogenization temperature (Thiery et al., 1994), and overall pressure estimation – by using computation programs of Bakker (2003).

*****The minimum trapping pressure estimated using the data on vapor bubble disappearance and halite dissolution (Roedder, 1984).

Table 7. Combined Gas and Leachate Analyses of Fluid Inclusions in Quartz from the Lermontovskoe Deposit (as Determined by Bulk Gas Chromatography, Ion Chromatography, and ICP-MS Analysis of Leachate)

Hydrothermal stages	Hydrosilicate alteration			Phyllic alteration					
				Early (quartz-muscovite-carbonate-arsenopyrite-apatite-scheelite) assemblage			Late (quartz-sericite-carbonate-sulfide-Bi-Au) assemblage		
samples	1	2	3	4	5	6	7	8	9
H_2O, ppm	697.90	1008.23	898.13	1443.94	905.57	1512.02	1489.82	763.44	1052.45
Major components, grams per kilogram H_2O									
CO_2	26.20	14.51	5.64	23.41	13.51	8.81	7.40	8.21	26.71
CH_4	5.21	9.10	8.21	2.26	5.88	2.44	2.22	2.08	1.56
Cl^-	5.35	4.33	3.60	4.56	3.22	19.93	4.03	3.67	11.22
F^-	<0.7	<0.4	<0.4	<0.2	<0.5	<0.4	<0.3	<0.4	<0.5
SO_4^{2-}	7.49	6.64	7.42	2.49	2.11	2.20	0.61	0.62	0.52
HCO_3^-	13.99	5.62	6.11	7.24	10.21	7.56	6.88	8.30	12.44
B^{3-}	0.11	0.21	0.22	0.04	0.08	0.06	0.03	0.04	0.09
Na^+	3.38	4.80	4.31	2.07	3.90	2.77	2.54	3.22	5.24
K^+	0.48	0.83	0.52	0.37	0.46	0.19	0.14	0.08	0.12
Ca^{2+}	1.85	4.22	3.78	1.92	1.76	2.11	1.26	1.16	1.19
Mg^{2+}	3.44	5.61	4.27	1.40	1.32	0.64	0.77	0.62	0.41
Mole fractions (major cations and anions)									
Na^+	0.42	0.37	0.39	0.44	0.60	0.60	0.61	0.71	0.82
K^+	0.04	0.04	0.03	0.05	0.05	0.03	0.01	0.01	0.01
Ca^{2+}	0.13	0.19	0.20	0.23	0.16	0.26	0.18	0.15	0.11
Mg^{2+}	0.41	0.41	0.38	0.28	0.19	0.12	0.19	0.13	0.06
Cl^-	0.33	0.50	0.44	0.47	0.35	0.71	0.48	0.44	0.61
HCO_3^-	0.50	0.28	0.30	0.43	0.65	0.29	0.49	0.56	0.39
Mole ratios									
CO_2/CH_4	1.8	0.6	0.2	3.8	0.8	1.3	1.2	1.4	6.1
Na/K	11.9	10.2	14.6	8.8	13.2	23.7	42.4	53.4	88.2
Na+K/Ca+Mg	0.8	0.7	0.7	0.9	1.8	1.7	1.7	8.4	4.9
HCO_3/Cl	1.5	0.7	1.0	0.9	1.8	4	1.0	0.6	0.6

Samples: 1-3 – quartz from hydrosilicate (amphibole-chlorite-quartz-pyrrhotite-scheelite) alteration zone overprinting skarns, 4-6 - quartz from the early (quartz-muscovite-carbonate-arsenopyrite-apatite-scheelite) assemblage of phyllic alteration, 7-9 – quartz from the late (quartz-sericite-carbonate-sulfide-Bi-Au) assemblage of phyllic alteration.

Table 8. Sulfur isotope compositions of sulfides from the Lermontovskoe deposit

Samples	Description	Po*	Po	Ccp	Apy	Sph	Py
		$\delta^{34}S_{VCDT}$, ‰					
Hydrosilicate alteration							
L-39	Quartz and amphibole, abundant scheelite, minor pyrrhotite and chalcopyrite	-7.5		-6.9			
L364/76	Quartz and amphibole, abundant scheelite, minor pyrrhotite and chalcopyrite	-7.0		-6.8			
L-56	Quartz and amphibole, abundant scheelite, minor pyrrhotite and chalcopyrite	-7.2		-6.9			
L-104	Quartz and amphibole, abundant pyrrhotite, minor scheelite and chalcopyrite	-7.3		-7.3			
L-46	Quartz and amphibole, abundant pyrrhotite, minor scheelite and chalcopyrite		-6.0				
L-47	Quartz and amphibole, abundant pyrrhotite and scheelite		-6.0				
Phyllic alteration							
Early (quartz-muscovite-carbonate-arsenopyrite-apatite-scheelite) assemblage							
L-004	Quartz-muscovite-carbonate veinlet with abundant coarse-grained arsenopyrite				-5.4		
L-14	Quartz-muscovite-carbonate veinlet with abundant coarse-grained arsenopyrite				-5.4		
L-15	Quartz-muscovite-carbonate veinlet with abundant arsenopyrite and scheelite, minor apatite				-5.6		
L-17	Quartz-muscovite-carbonate veinlet with minor arsenopyrite and abundant scheelite				-5.4		
L-22	Quartz-muscovite-carbonate veinlet with minor fine-grained arsenopyrite and scheelite				-5.5		
L-005	Quartz-muscovite-carbonate veinlet with minor arsenopyrite, abundant apatite and scheelite				-5.4		
L-007	Quartz-muscovite-carbonate veinlet with minor arsenopyrite, abundant apatite and scheelite				-5.3		
Late (quartz-sericite-carbonate-sulfide-Bi-Au) assemblage							
L-38	Quartz-sericite-carbonate veinlet with minor pyrrhotite and chalcopyrite, trace scheelite		-5.5				
L-40	Quartz-sericite-carbonate veinlet with minor pyrrhotite and chalcopyrite, trace scheelite		-5.0				
L-002	Quartz-sericite-carbonate veinlet with minor pyrrhotite and sphalerite, trace scheelite					-5.5	
L361/76	Quartz-sericite-carbonate veinlet with minor pyrrhotite and sphalerite, trace scheelite					-4.5	
L-103	Quartz-sericite-carbonate veinlet with minor sphalerite and scheelite, trace pyrrhotite					-4.5	
L-24	Quartz-sericite-carbonate veinlet with minor sphalerite and scheelite, trace pyrrhotite					-4.4	
L-29	Quartz-sericite-carbonate veinlet with minor sphalerite and pyrite, trace scheelite					-4.4	-4.5
L-30	Quartz-sericite-carbonate veinlet with minor sphalerite and pyrite, trace scheelite					-4.4	-4.5

Abbreviations: Po – monocline pyrrhotite, Po* – hexagonal pyrrhotite (non-magnetic); Ccp – chalcopyrite, Apy – arsenopyrite, Sph – sphalerite, Py - pyrite.

Highlights

The deposit is an example of reduced-type W skarn related to high-K peraluminous igneous suite
Two to three major stages of scheelite and sulfide deposition occurred
Fluid evolution included incursions of high-salinity NaCl-dominated, and essentially carbonic fluids
The deposit represents a root leves of reduced intrusion-related W-Au deposits